

Phosphasalalen Rare-Earth Complexes for the Polymerization of *rac*-Lactide and *rac*- β -Butyrolactone

Hui Liu and Xiaochao Shi*

Cite This: *Inorg. Chem.* 2021, 60, 705–717

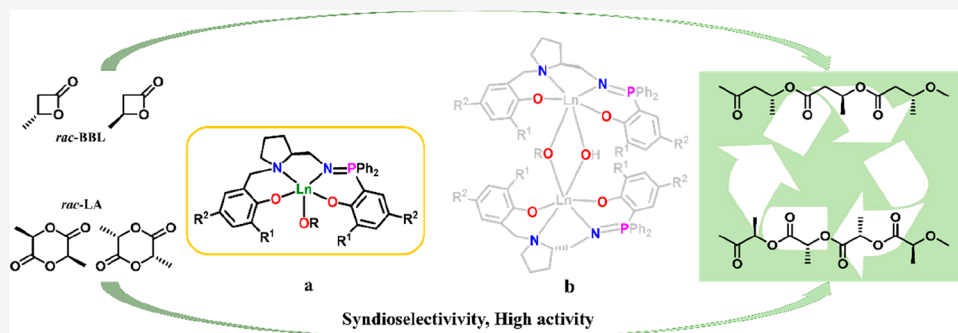
Read Online

ACCESS |

Metrics & More

Article Recommendations

Supporting Information



ABSTRACT: A series of new phosphasalalen pro-ligands, analogues of salalen but with an iminophosphorane replacing the imine functionality, and their corresponding rare-earth alkoxide and siloxide complexes were synthesized. The multinuclear NMR spectra and X-ray diffraction analyses revealed that, for the *tert*-butoxide and ethoxide complexes, the resulting phosphasalalen rare-earth product was composed of a mononuclear alkoxide and a binuclear complex containing bridged alkoxy and hydroxy groups, while an analogous binuclear complex was isolated as the sole product for the siloxide complex. All the complexes could catalyze the heteroselective ring-opening polymerization (ROP) of *rac*-lactide (P_r up to 0.77) with high catalytic activities and a controlled polydispersity. Remarkably, the yttrium and lutetium phosphasalalen complexes could also efficiently catalyze the ROP of *rac*- β -butyrolactone to produce syndiotactic polymers (P_r up to 0.73) while their salalen analogues were inert, revealing the special effects of the iminophosphorane moiety. Detailed end-group analyses and kinetic investigations suggested that the alkoxy–hydroxy-bridged complexes maintained their binuclear structures in the polymerization.

INTRODUCTION

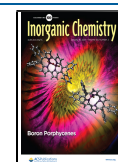
The environmental issues regarding plastic waste have attracted much attention to the development of biodegradable and biocompatible polymers that can decompose quickly without harming the organisms and environment.¹ As polymeric alternatives, aliphatic polyesters, such as poly(lactides) (PLA) and poly(3-hydroxybutyrate) (PHB), are among the most promising ecologic materials and have excellent applications in the fields of packaging, agriculture, biomedical research, etc.^{1,2} The metal-catalyzed ring-opening polymerizations (ROP) of *rac*-lactide (*rac*-LA) and *rac*- β -butyrolactone (*rac*-BBL) represent a promising way to access these polymers, especially involving the control of the stereoreactivity. Nowadays, a wide range of metal catalysts have been developed to produce different stereospecific PLAs and PHBs;^{3,4} the rare-earth (Ln) catalysts are among those receiving most intensive investigations due to their high catalytic activities, high degrees of stereocontrol, and the ability to control the microstructures of polymers by reasonably modifying the ancillary ligands as well as choosing the metal centers.^{5–8} The amine-bridged bis-(phenolate)s pro-ligands were proven to be extremely effective, and their yttrium complexes have been widely investigated as

syndiospecific catalysts for the polymerization of *rac*-LA or *rac*-BBL with outstanding activities and stereoselectivities to produce highly heterotactic PLA (P_r up to 0.99) and highly syndiotactic PHBs (P_r up to 0.94). The Williams group has also described a series of phosphasalalen rare-earth complexes, some of which exhibited high catalytic activities and a tolerance for low catalyst loadings with excellent polymerization control.⁸ The impressive catalytic performance of rare-earth complexes for the ROP of *rac*-LA and *rac*-BBL encouraged continuous efforts in this field for further enhancement.

Salalens (Figure 1C), combining half salalen (Figure 1A) and half salan (Figure 1B) pro-ligands in a hybrid mold, are [ONNO]-type tetradentate pro-ligands that include imine- and

Received: September 14, 2020

Published: January 6, 2021



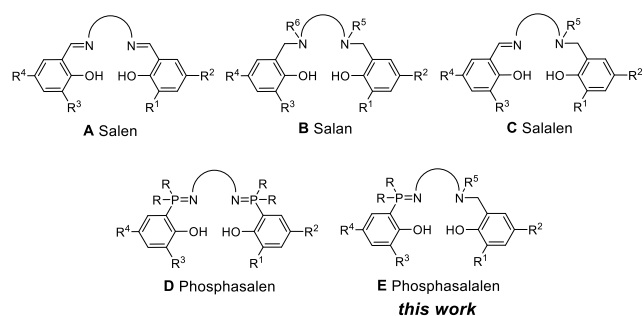


Figure 1. General structure of [ONNO]-type tetradentate pro-ligands.

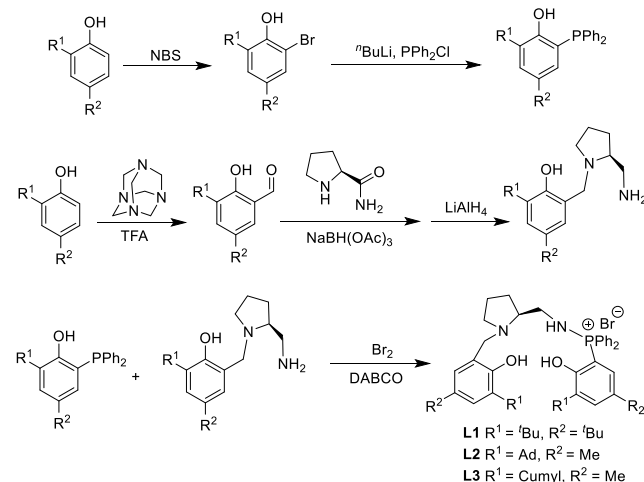
amine-neutral donors and two phenolate arms. Their corresponding metal complexes have been used successfully in the polymerization of diverse monomers, such as the stereoselective ROP of *rac*-LA, the copolymerization of epoxides with carbon dioxide, and the isospecific polymerization of α -olefin.^{9–11} Surprisingly, heteroatomic substitutions on the backbone of salalen pro-ligands have been less investigated; only a few sulfur-substituted pro-ligands were reported, and in some the sulfur atom did not coordinate to the metal centers.¹² On the other hand, the iminophosphorane moieties behave as strong σ - and π -donors due to the presence of two lone pairs at the nitrogen atom and the lack of π -accepting ability, respectively. With different steric and electronic properties imposed on the imine moieties, the iminophosphorane moieties are of great interest and are well established in coordination and catalytic chemistry.¹³ The phosphasalalen pro-ligands (Figure 1D), referring to the iminophosphorane-substituted salen pro-ligands, have attracted intensive research attentions, and their metal complexes exhibited rather different catalytic performances when compared with their salen analogues.^{8,13a,14} The success of iminophosphorane moieties in ligand designs prompted us to modify the versatile salalen pro-ligands by introducing an iminophosphorane moiety. We envisage that the incorporation of an iminophosphorane moiety to the normal salalen backbone will result in a new kind of pro-ligand, namely phosphasalalen (Figure 1E), and the corresponding metal (e.g., rare-earth metal) complexes would exhibit interesting catalytic properties in various applications (e.g., the ROP of *rac*-LA and *rac*-BBL).¹⁵

Herein, we report a new family of phosphasalalen pro-ligands containing a chiral rigid pyrrolidine framework and their rare-earth complexes for the syndiospecific polymerization of *rac*-LA and *rac*-BBL. The NMR spectra demonstrated that the synthesized rare-earth mixtures contained mainly the mononuclear alkoxide complex and a minor binuclear complex with bridged alkoxo and hydroxo groups. All the complexes were highly active catalysts for the heterospecific ROP of *rac*-LA. Interestingly, the phosphasalalen complexes could also serve as efficient catalysts for the ROP of *rac*-BBL while their salalen analogues were inert, revealing the considerable role of the iminophosphorane functionality in the structure–reactivity relationship.

RESULTS AND DISCUSSION

Synthesis and Characterization of Complexes. The phosphasalalen pro-ligands L1–L3 with chiral pyrrolidine backbones were handled as stable bromine salts, and their synthetic routes are outlined in Scheme 1. The reagents,

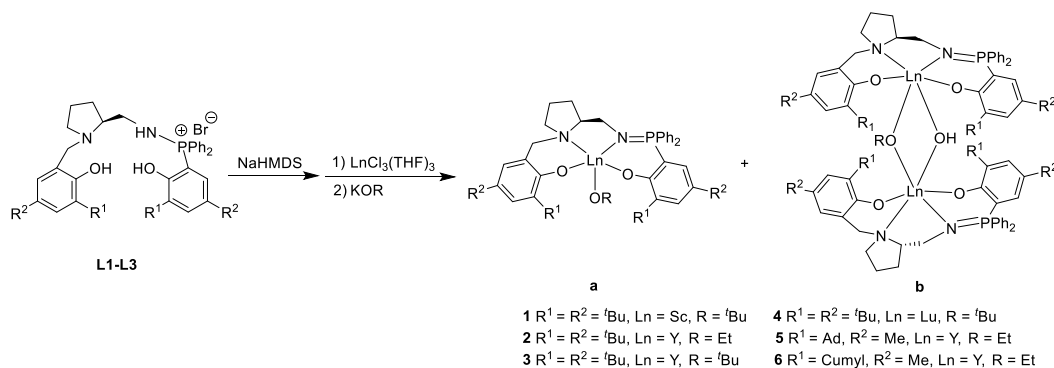
Scheme 1. Synthesis of Phosphasalalen Pro-Ligands



namely phosphinophenols and aminopyrrolidinylphenols with bulky substituents at the *ortho*-phenoxide positions, were prepared following the literature procedures.¹⁶ The corresponding phosphonium bromide salts, prepared by the oxidation of phosphinophenol with liquid bromine in situ, were reacted with equimolar amounts of aminopyrrolidinylphenols via a Kirsanov reaction in the presence of 1,4-diazabicyclo[2.2.2]octane (DABCO) to efficiently give the desired phosphasalalen pro-ligands L1–L3 (Scheme 1, Ad = adamantanyl and Cumyl = 2-phenylpropan-2-yl). The pro-ligand L1 was purified by recrystallization from its Et₂O solution, while L2 and L3 were purified by column chromatography on silica gel (CH₂Cl₂/MeOH). The pure phosphasalalen pro-ligands were obtained with around 50% yields as white powders that were stable in the presence of oxygen and moisture, and all the new pro-ligands were fully characterized by multinuclear NMR spectroscopy (¹H, ¹³C and ³¹P NMR, Figures S1–S9).

The deprotonation of L1–L3 with 3 equiv of sodium bis(trimethylsilyl)amide generated the corresponding sodium salts; the reaction was monitored using ³¹P NMR spectroscopy, which showed obvious chemical shifts as singlet signals, such as shifts from δ 44.87 to 21.61 ppm for L1 (Figures S3 and S17). The reaction of the sodium salts of ligands with LnCl₃(THF)_x at a low temperature (–30 °C) to form the rare-earth phosphasalalen chloride complexes (from δ 21.61 ppm for the sodium salt of L1 to δ 34.33 ppm for its corresponding phosphasalalen yttrium chloride in ³¹P{¹H} NMR spectra, Figure S19), led to formation of the phosphasalalen metal alkoxide mixtures 1–6 in Scheme 2 following the addition of potassium alkoxides (ethoxide and *tert*-butoxide). In the ³¹P{¹H} NMR spectra of 1–6, two peaks with the a relative ratio of integrations around 9:1 (except around 8:2 for 5) were observed, suggesting that each mixture contained two different complexes. To clarify the detailed structures of both complexes, we took mixture 3 as an example to investigate in detail. The peaks at δ 36.94 (major) and 33.32 ppm (minor) in the ³¹P{¹H} NMR spectrum had a ratio of 10:1 in integration; in the ¹H NMR spectrum, the peak assigned for the –O^tBu group possessed equal integration to each of the four discrete peaks assigned for the *tert*-butyl substituents in ligand L1. The ¹³C{¹H} NMR spectrum showed a single set of equivalent doublets at δ 167.4 ppm, which was assigned for the quaternary phosphine-attached phenolate carbon atom (see

Scheme 2. Synthesis of Phosphasalalen Rare-Earth Complexes 1–6



Figures S20–S22). All the data suggested that the major component, namely **3a**, possessed a mononuclear structure with the coordination of one ligand and one $-\text{O}^t\text{Bu}$ group (Scheme 2).^{8a} Furthermore, we fortunately obtained the crystal structure of **3b**, which was the minor component in **3**, revealing the binuclear ^tbutoxo–hydroxo-bridged structure of **3b** (Figure 2). The multinuclear NMR spectra of the

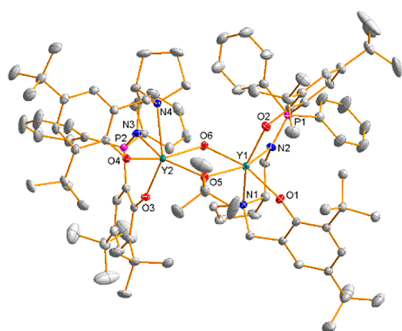


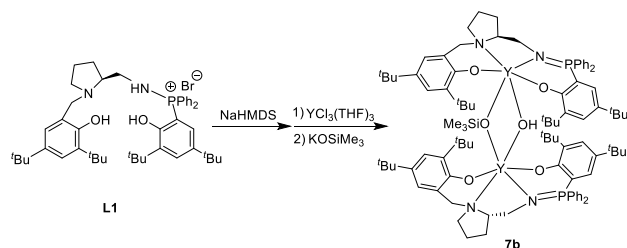
Figure 2. Molecular structure of complex **3b** (thermal ellipsoids are shown at the 30% probability level). Hydrogen atoms were omitted for clarity. Selected bond distances (Å) and angles (°) are as follows: Y1–O1, 2.159(2); Y1–O2, 2.135(2); Y1–O5, 2.297(2); Y1–O6, 2.258(2); Y1–N1, 2.525(2); Y1–N2, 2.383(3); Y2–O3, 2.154(2); Y2–O4, 2.159(2); Y2–O5, 2.304(2); Y2–O6, 2.243(2); Y2–N3, 2.544(3); Y2–N4, 2.376(3); O1–Y1–N1, 76.45(8); O2–Y1–N2, 80.65(9); N2–Y1–N1, 71.83(10); O1–Y1–O5, 106.46(9); O2–Y1–O6, 102.56(9); O5–Y1–O6, 71.23(7); O3–Y2–N3, 76.26(8); O4–Y2–N4, 80.84(9); N3–Y2–N4, 70.45(9); O3–Y2–O5, 105.37(8); O4–Y2–O6, 100.39(9); and O5–Y2–O6, 71.34(8).

crystalline solid of **3b** (δ 33.32 ppm in $^{31}\text{P}\{^1\text{H}\}$ NMR spectrum) convinced us of the mononuclear structure of **3a** (Figures S23–S26). A solution DOSY NMR experiment was also used to compare the hydrodynamic radii of complexes **3a** and **3b** with those estimated from the DFT calculations and X-ray crystal structure, respectively (see Figure S44 for details). The solution hydrodynamic radii of complexes **3a** and **3b** were determined to 15.09 and 20.52 Å, respectively (C_6D_6 , 25 °C). The radius determined from the crystal structure of complex **3b** was 21.250 Å, which was very close to that determined from the DOSY NMR spectrum (20.52 Å). For complex **3a**, the DFT calculations (computed at B3LYP and 3-21g*) of the optimized geometry showed a radius of 15.825 Å, which was in agreement with that determined by the DOSY NMR analysis (15.09 Å). Thus, the DOSY NMR evidence also supported the mononuclear structure of complex **3a**. However, we could not obtain the pure complex **3a** despite having enough evidence in

the multinuclear NMR spectra for its formation and the low content of **3b**.

We failed to realize the transformation of **3a** to **3b** by heating mixture **3** at 70 °C or adding a controlled amount of water ($n(\text{H}_2\text{O}):n(\text{Y}^{3+}) = 0.5$), implying that the formation of the binuclear complex **3b** proceeded in an unexpected way.¹⁶ No evidence indicating the formation of a binuclear complex with two bridged $-\text{O}^t\text{Bu}$ groups has ever been observed, since the ^1H NMR spectra of **3** had no differences in a wide operating temperature ranging from -80 to 60 °C in $\text{THF}-d_8$ (Figures S42–S43). When more bulky ligands **L2** and **L3** were used, the resultant mixtures **5** and **6** could be also obtained, and the mononuclear structure was identified as the major component. However, $^{31}\text{P}\{^1\text{H}\}$ NMR spectra revealed higher ratios of binuclear complexes compared to **3**, which were 22.4% in **5** and 16.6% in **6** (Figures S32 and S35, respectively). These suggested that the steric hindrance of the ligands played an important role in the formation of the binuclear complexes. Interestingly, when a bulkier and more easily decomposed $-\text{OSiMe}_3$ group was used as a coordinated group, the multinuclear NMR spectrum demonstrated that the binuclear complex **7b** was the sole product (Scheme 3), giving evidence

Scheme 3. Synthesis of Phosphasalalen Rare-Earth Complex 7b



of another important factor to form the binuclear complexes. On the basis of the above experimental findings, we reasoned the formation of binuclear hydroxo-bridged complexes was mainly due to the rigid inheritance and steric congestion of the ligands as well as the unusual O–C or O–Si bond cleavage of the $-\text{OR}$ groups, which might accompany the hydrogen abstraction of solvent.¹⁷

Single crystals of the binuclear complexes **3b**, **6b**, and **7b** suitable for single-crystal X-ray diffractions were isolated from their *n*-hexane solutions, and the molecular structures of the complexes as well as the selected bond lengths and bond angles are depicted in Figures 2–4, respectively. As shown in the molecular structures of these complexes, the rigidity of the

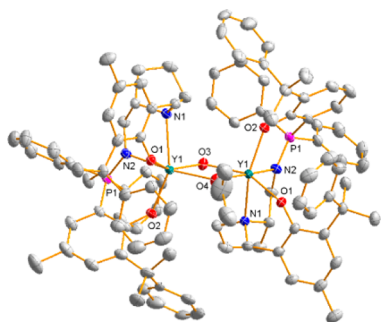


Figure 3. Molecular structure of complex **6b** (thermal ellipsoids are shown at the 30% probability level). Hydrogen atoms were omitted for clarity. Selected bond distances (Å) and angles (°) are as follows: Y1–O1, 2.159(3); Y1–O2, 2.197(3); Y1–O3, 2.247(3); Y1–O4, 2.257(3); Y1–N1, 2.501(4); Y1–N2, 2.396(4); O1–Y1–N1, 78.49(13); O2–Y1–N2, 80.17(14); N2–Y1–N1, 69.53(13); O3–Y1–O4, 71.83(14); O1–Y1–O3, 153.75(10); and O4–Y1–N2, 168.87(14).

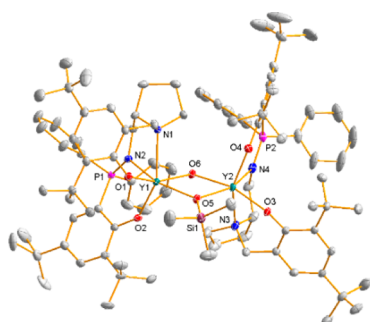


Figure 4. Molecular structure of complex **7b** (thermal ellipsoids are shown at the 30% probability level). Hydrogen atoms were omitted for clarity. Selected bond distances (Å) and angles (°) are as follows: Y1–O1, 2.165(2); Y1–O2, 2.154(2); Y1–O5, 2.3123(19); Y1–O6, 2.247(2); Y1–N1, 2.533(3); Y1–N2, 2.373(2); Y2–O3, 2.154(2); Y2–O4, 2.135(2); Y2–O5, 2.310(2); Y2–O6, 2.253(2); Y2–N3, 2.509(3); Y2–N4, 2.375(3); O1–Y1–N1, 76.92(8); O2–Y1–N2, 80.91(8); N2–Y1–N1, 70.61(8); O1–Y1–O5, 103.42(8); O2–Y1–O6, 99.97(8); O5–Y1–O6, 72.09(8); O3–Y2–N3, 77.31(8); O4–Y2–N4, 80.76(9); N3–Y2–N4, 99.72(9); O3–Y2–O5, 103.67(8); O4–Y2–O6, 103.10(8); and O5–Y2–O6, 72.03(7).

pyrrolidine backbone has no influences on the coordination of atoms; however, its inherent chirality induces the bulky aminoiminophosphorane moiety to form a rather crowded configuration around the Ln–OH group. The phosphasalalen ligands bind to the metal centers with two oxygen atoms, one imine atom from the iminophosphorane, and one amine atom from pyrrolidine, and the four coordinated atoms wrap diastereospecifically in the *fac-mer* mode in both complexes. Each metal center exhibits a distorted octahedral geometry formed by the tetradentate phosphasalalen ligand and the alkoxo and hydroxo bridges, revealing clearly that the complexes adopt a binuclear structure in the solid state. Moreover, the two related metal centers and the bridged alkoxo and hydroxo groups construct a [Ln₂O₂] four-membered ring, and the quaternion ring is in a nearly perfect plane. The distances of the two metal centers to the corresponding coordinated atoms are very close in the complexes, e.g., the bond lengths of Y–O (pyrrolidine-side phenolate) in complex **3b** are 2.159(2) (Y1–O1) and 2.154(2) Å (Y2–O3); the coordination geometries around

the two metal centers are also similar. The ³¹P{¹H} NMR spectrum of complex **3b** exhibits a singlet signal at room temperature (δ 33.32 ppm), suggesting the similar coordination environments of the two phosphorus atoms. As expected, the bond lengths of Y–N (pyrrolidine) are longer than those of Y–N (iminophosphorane), and all the bond lengths of Y–N are in accordance with the values from previous results.^{14,15,18} The bond lengths of Y–O (O^tBu) are 2.297(2) and 2.304(2) Å, which are slightly longer than those of Y–O (OH) (2.258(2) and 2.243(2) Å, respectively; this could be attributed to the steric hindrance of the bulky –O^tBu ligand. The bond angles of O(Ar)–Y–N (pyrrolidine) (76.45(8)° and 76.26(8)°) are smaller than those of O(Ar)–Y–N (iminophosphorane) (80.65(9)° and 80.84(9)°), which is attributed to the rigidity of the iminophosphorane moiety. The bond lengths and bond angles in complexes **6b** and **7b** have the same tendency as those in complex **3b**, and the corresponding parameters in **6b** and **7b** are also comparable to those of **3b**.

Ring-Opening Polymerization of *rac*-LA and *rac*-BBL.

As our purpose for the design and synthesis of phosphasalalen ligands, **1–6** were tested for the stereospecific polymerization of *rac*-LA and *rac*-BBL to elucidate the structure–reactivity relationship. The representative polymerization results are summarized in Tables 1 and 2 for *rac*-LA and *rac*-BBL, respectively. Due to the special electronic effect of the iminophosphorane moiety with a strong σ - and π -donating capability, the phosphasalalen rare-earth precursors **1–6** showed high catalytic activities for the polymerization of *rac*-LA (P_r up to 0.77). Remarkably, the yttrium and lutetium phosphasalalen mixtures **2–6** could also efficiently catalyze the syndioselektiv polymerization of *rac*-BBL (P_r up to 0.73), whereas their corresponding salalen analogues were inactive.¹⁵

All the complexes could catalyze the *rac*-LA polymerization in the absence of other chain transfer agents or coactivators. Prominent solvent effects were observed in the polymerization results, of which a polar solvent was beneficial for obtaining the polymer with a higher heteroselectivity. The phosphasalalen yttrium mixture **3** could serve as a highly efficient catalyst for the ROP of *rac*-LA, and converted 200 equiv of monomers nearly quantitatively in 4 min (1 M *rac*-LA solution in THF) to give a polylactide with a high molecular weight ($M_n = 37.0$ kDa, $M_w/M_n = 1.07$) and good heteroselectivity ($P_r = 0.72$). The high catalytic activity enabled **3** to catalyze 2000 equiv of *rac*-LA with a conversion of 70% in 120 min (entry 9 in Table 1). These results showed that the yttrium phosphasalalen complexes were among the most efficient yttrium catalysts for the polymerization of *rac*-LA.⁵ Compared to the salalen yttrium analogue, **3** exhibited a comparable catalytic activity but lower stereoselectivity ($P_r = 0.72$ for **3** vs $P_r = 0.85$ for the salalen yttrium complex under similar polymerization conditions) in the ROP of *rac*-LA.¹⁵ When the central metal was a scandium ion with a small radius, **1** showed a much lower catalytic activity (entry 1 in Table 1). This could be partly attribute to the bulky phosphasalalen ligand and the subsequent compaction in space around the smaller Sc³⁺ center, which was unfavored for the coordination and insertion of lactide monomers. The lutetium phosphasalalen mixture **4** showed a comparably catalytic performance to that of **3**. Surprisingly, the coordinated alkoxide anions had an inconceivable influence on the catalytic activity; the yttrium mixture **3** with *tert*-butoxide had a much higher catalytic activity than **2** with an ethoxide, which differs from the

Table 1. Data for the ROP of *rac*-LA Using the Phosphasalalen Rare-Earth Catalysts^a

entry	cat.	[I]:[LA]	<i>t</i> (min)	con. (%) ^b	<i>M_n</i> (kDa) ^c	<i>M_{n,calc}</i> (kDa) ^d	<i>M_w</i> / <i>M_n</i> ^c	<i>P_r</i> ^e
1	1	1:200	50	72	22.6	20.8	1.03	0.66
2	2	1:200	40	98	17.2	28.3	1.03	0.67
3	2	1:500	90	87	32.1	62.7	1.24	0.69
4	3	1:200	4	99	37.0	28.6	1.07	0.72
5 ^f	3	1:200	4	98	40.9	28.3	1.05	0.62
6 ^g	3	1:200	4	98	37.6	28.3	1.06	0.62
7	3	1:500	14	97	62.7	70.0	1.10	0.69
8	3	1:1000	36	97	101.6	139.9	1.25	0.73
9	3	1:2000	120	70	103.8	201.9	1.30	0.70
10	4	1:200	4	96	38.4	27.7	1.03	0.69
11	5	1:200	90	97	24.6	28.0	1.11	0.75
12	6	1:200	90	98	26.1	28.3	1.15	0.76
13	3b	1:200	4	98	26.1	28.3	1.05	0.63
14	6b	1:200	80	89	25.9	25.7	1.06	0.77
15	7b	1:200	120	99	18.5	28.6	1.08	0.68

^aAll reactions were carried out at room temperature (25 °C), [LA] = 1 M, and with tetrahydrofuran (THF) as the solvent. ^bConversion was determined from the ¹H NMR spectra (CDCl₃) of crude polymers by integrating the methine resonance (*rac*-LA, δ 4.98–5.06 ppm; PLA, δ 5.08–5.22 ppm). ^cDetermined by SEC in THF using polystyrene as the standard. ^d*M_{n,calc}* = 144.13 × [LA]/[I] × (polymer conversion) (%) + 73.06 (–O^tBu)/45.06 (–OEt). ^eDetermined by the analysis of the tetrad signals in the methine region of the homodecoupling ¹H NMR spectrum at 25 °C. ^fDichloromethane (DCM) was used as the solvent. ^gToluene was used as the solvent.

Table 2. Data for the ROP of *rac*-BBL Using the Phosphasalalen Rare-Earth Catalysts^a

entry	cat.	[BBL]	[I]:[BBL]	<i>t</i> (h)	con. (%) ^b	<i>M_n</i> (kDa) ^c	<i>M_{n,calc}</i> (kDa) ^d	<i>M_w</i> / <i>M_n</i> ^c	<i>P_r</i> ^e
1	2	2 M	1:200	4	96	12.7	16.6	1.04	0.69
2	2	2 M	1:400	10	80	22.6	27.6	1.13	0.63
3	2	2 M	1:600	22	82	25.8	42.4	1.10	0.60
4	2	2 M	1:800	32	92	31.9	63.4	1.14	0.63
5	3	1 M	1:200	4	98	19.1	16.9	1.16	0.73
6	3	2 M	1:200	4	97	14.9	16.8	1.05	0.73
7	3	2 M	1:400	8	91	22.4	31.4	1.21	0.72
8	3	2 M	1:600	18	90	26.6	46.6	1.11	0.70
9	3	2 M	1:800	26	89	35.0	61.4	1.13	0.67
10	3	4 M	1:200	3	90	19.9	15.6	1.19	0.68
11 ^f	3	2 M	1:200	4	98	20.6	16.9	1.16	0.59
12 ^g	3	2 M	1:200	4	96	21.4	16.6	1.08	0.66
13	3	2 M (0 °C)	1:200	12	-	-	-	-	-
14	3	2 M (50 °C)	1:200	10	94	24.5	16.3	1.10	0.65
15	4	2 M	1:200	4	97	10.3	16.8	1.07	0.58
16	4	2 M	1:600	20	92	21.5	47.6	1.20	0.57
17	5	2 M	1:200	4	88	14.1	15.2	1.09	0.43
18	5	2 M	1:600	24	82	30.6	42.4	1.14	0.42
19	6	2 M	1:200	4	98	13.8	16.9	1.11	0.64
20	6	2 M	1:600	22	93	30.6	48.1	1.08	0.62
21	3b	2 M	1:200	4	94	20.8	16.3	1.18	0.66
22	6b	2 M	1:200	5	97	20.7	16.7	1.16	0.54
23	7b	2 M	1:200	20	94	17.3	16.3	1.13	0.62
24	1	2 M	1:200	24					

^aGeneral polymerization conditions are as follows: toluene as the solvent, at room temperature (25 °C), and the polymerization time was not optimized. ^bConversion of *rac*-BBL as determined by a ¹H NMR analysis of the crude polymer by integrating the methine resonance (CDCl₃; *rac*-BBL, δ 1.50–1.54 ppm; PHB, δ 1.25–1.31 ppm). ^cDetermined by SEC in THF using polystyrene as the standard. ^d*M_{n,calc}* = 86.09 × [BBL]/[I] × (polymer conversion) (%) + 45.06 (–OEt)/73.06 (–O^tBu)/89.19 (–OSiMe₃). ^e*P_r* is the probability of racemic linkages between monomer units measured by ¹³C NMR spectroscopy at 25 °C in CDCl₃. ^fTHF was used as the solvent. ^gDCM was used as the solvent.

previous observation that a smaller alkoxide group improved the activity due to its higher initiation rate of the *rac*-LA polymerization (entries 2–3, respectively, in Table 1).⁸ This might be attributed to the steric interaction between the alkoxide group and the *ortho*-phenolate group, which renders the bulky *tert*-butoxide more active than the ethoxide in regard to initiating the polymerization. The mixtures 5 and 6 with

ethoxide also showed lower activities than that of 3 but with a similar heteroselectivity. The binuclear complexes 3b and 6b showed comparable catalytic activities to those of 3 and 6, respectively. Due to the low content of the binuclear complex in 1–6, it is reasonable to conclude that the monomeric complex played a predominate role in the ROP of *rac*-LA.

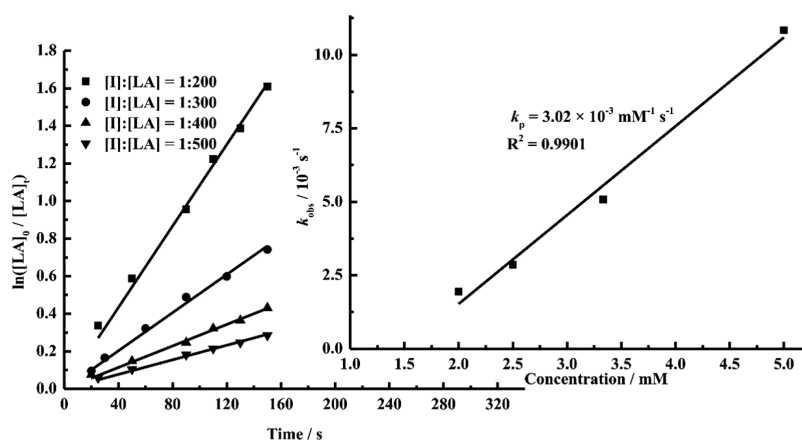


Figure 5. (Left) Plot showing first-order kinetic plots of $\ln([LA]_0/[LA]_t)$ vs time (s) for the polymerization of *rac*-LA catalyzed by **3** in THF at 25 °C and $[LA]_0 = 1$ M. $[I]:[LA] = 1:200$, $k_{obs} = 10.84 \times 10^{-3} \text{ s}^{-1}$, $R^2 = 0.9927$; $[I]:[LA] = 1:300$, $k_{obs} = 5.08 \times 10^{-3} \text{ s}^{-1}$, $R^2 = 0.9937$; $[I]:[LA] = 1:400$, $k_{obs} = 2.86 \times 10^{-3} \text{ s}^{-1}$, $R^2 = 0.9928$; and $[I]:[LA] = 1:500$, $k_{obs} = 1.94 \times 10^{-3} \text{ s}^{-1}$, $R^2 = 0.9926$. (Right) Plot of k_{obs} vs $[I]$ for the calculation of the propagation rate constant k_p with polymerization conditions of THF, 25 °C, $[LA]_0 = 1$ M, and $[3] = 2\text{--}5$ mM.

Complex **7b** with a $-\text{OSiMe}_3$ group could also quantitatively convert 200 equiv of *rac*-LA in 120 min.

All the resultant PLAs catalyzed by phosphasalalen rare-earth catalysts had high molecular weights and narrow molecular weight distributions ($M_w/M_n \leq 1.30$), suggesting that the polymerization proceeded in a controlled manner. In the *rac*-LA ROP catalyzed by **3**, a first-order dependence of the conversion rate on the lactide concentration was observed, as evidenced by the linear fits to the plot of $\ln([LA]_0/[LA]_t)$ vs time (Figure 5). From the k_{obs} values determined over a range of different catalyst concentrations, the reaction also had a first-order dependence on the catalyst concentration. Thus, the overall rate law is second-order with the propagation rate constant at $k_p = 3.02 \times 10^{-3} \text{ mM}^{-1} \text{ s}^{-1}$. The first-order dependence on both the lactide and catalyst concentrations was also reported by the phosphasalalen rare-earth complexes.^{8d}

In addition to the excellent activity for the polymerization of *rac*-LA, the phosphasalalen yttrium and lutetium complexes **2–6** could also effectively catalyze the ROP of *rac*-BBL at room temperature; the summary of polymerization results is shown in Table 2. Toluene was the optimal solvent for this polymerization, and the monomer concentration slightly influenced the catalytic property in our trials; a moderate 2 M concentration was selected for further investigations (entries 5, 6, and 10 in Table 2). Under these conditions, **3** could nearly complete the polymerization of 200 equiv of *rac*-BBL in 4 h to give the polymer with a high molecular weight ($M_n = 14.9$ kDa), a narrow polydispersity ($M_w/M_n = 1.05$), and a moderate syndioselectivity ($P_r = 0.73$). The lutetium mixture **4** could also convert 200 equiv of monomer in a conversion of 96%; however, the tacticity of the resultant polymer ($P_r = 0.58$) was much lower than that of the polymer produced by the yttrium analogue ($P_r = 0.73$), implying the significant influence of metal centers in stereocontrol (entry 1 and 4, respectively, in Table 2). Similar to the influence of the alkoxide group in *rac*-LA polymerization, a bulky group was also beneficial to the catalytic activity in the polymerization of *rac*-BBL. For example, **3** with a *tert*-butoxide group could convert the monomer in a 91% conversion over 8 h, while there was an 80% conversion over 10 h for **2** containing an ethoxide with the monomer-to-feed ratio of 400 (entries 2 and 7, respectively, in Table 2). The pure binuclear complexes **3b** and **6b** could also promote the polymerization of *rac*-BBL

efficiently and converted 200 equiv of monomers in high conversions within 5 h; however, 20 h was needed for complex **7b**, implying the lower catalytic initiation efficiency of the trimethylsiloxy group. Moreover, the mixture **1** with central Sc^{3+} ions was inactive for the ROP of *rac*-BBL (entry 24 in Table 2). $^{13}\text{C}\{^1\text{H}\}$ NMR measurements were used to investigate the tacticity of the resulting PHBs. The methyl region displayed two peaks corresponding to the *r* and *m* diads at δ 169.34 and 169.21 ppm, respectively, indicating all the resultant PHBs were syndiotactic-enriched since the *r* diad was more abundant in most of the samples (except **5**, which gave slightly isotactic-enriched PHB). However, the calculated molecular weights of the resultant polymers (based on the monomer feed ratio and conversion) did not show a clear relationship with the experimental values for the number-averaged molecular weight. Despite of the presence of chiral pyrrolidine in the phosphasalalen rare-earth complexes, statistical analysis by the Bernoulli model triad test confirmed a chain-end control mechanism in the ROP of *rac*-BBL (Table S1), that is, the stereochemistry in the polymerization was controlled by the chirality of the last-inserted butyrolactone unit. Considering the fact that the corresponding salalen rare-earth complexes were inactive for the ROP of *rac*-BBL, we ascribed the efficiently catalytic performances of **2–6** to the crucial iminophosphorane moiety in phosphasalalen ligands. NBO (natural bond orbital) analyses proved the significant difference between the iminophosphorane moieties and the imine moieties in their divergent electronic properties (Figure 6). The charge difference between the phosphorus and the nitrogen atoms in an iminophosphorane moiety ($|\Delta q| = 2.94$) is much higher than that between the carbon and the nitrogen atoms in an imine moiety ($|\Delta q| = 0.49$). The Wiberg indexes of

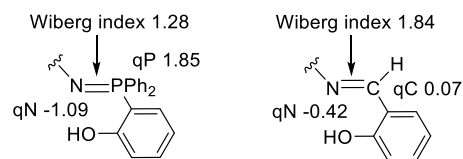


Figure 6. Comparison of the iminophosphorane and imine in Wiberg indexes and NBO charge calculated using Gaussian09 with the B3PW91 functional and 6-31+G* basis set.

the P–N and C–N bonds are 1.28 and 1.84, respectively. All of these indicate that the iminophosphorane adopts a dipolar structure (P^+-N^- instead of the conventional $P=N$) and is much more electron-donating than the imine.^{8a} It is well-known that, in the ROP of lactone, the high catalytic activity relies significantly on the efficient insertion of the lactone unit, thus requiring a labile metal alkoxide bond in the insertion step.^{8c,14a} Compared to the salalen ligands, the more electron-donating phosphasalalen ligand can decrease the Lewis acidity of the central yttrium and lutetium ions in 2–6 more significantly, benefiting the labilization of the metal-alkoxide bond and reducing the ring-opening energy of this β -butyrolactone attacked by the metal alkoxide; this could also explain the inactivity of 1 with a more Lewis acidic scandium center.

Due to the presence of two different bridged groups ($-O^tBu$ and $-OH$) in the complex 3b, it is important to clarify the real initiation group during the polymerization. The microstructures of the obtained oligomer of *rac*-BBL were evaluated by multinuclear NMR spectroscopy (Figure 7) and MALDI-

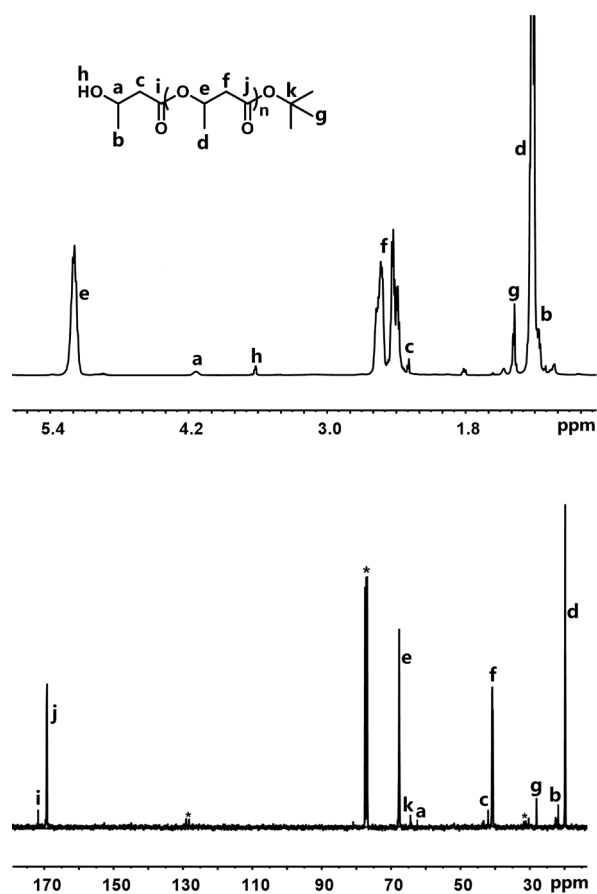


Figure 7. 1H and $^{13}C\{^1H\}$ NMR spectra ($CDCl_3$) of the PHB oligomer prepared from complex 3b. Conditions are as follows: $[BBL] = 2$ M, $[I]:[BBL] = 1:20$, toluene, and 25 °C.

TOF mass spectroscopy (Figure 8). The 1H NMR spectrum of the PHB oligomer, which was prepared by the catalyst 3b with the monomer in a 1:20 molar ratio, clearly demonstrated the expected PHB main chain structure, with δ 1.24 and 5.20 ppm assigned to the methyl and methine protons, respectively. The peak at δ 1.39 ppm could be assigned to the $-O^tBu$ en group, whereas the other end of the polymeric chain was found to be

a terminal hydroxybutyrate unit featuring peaks at δ 4.15 and 3.64 ppm in the 1H NMR spectrum.⁷ In the $^{13}C\{^1H\}$ NMR spectrum, the end-group analysis confirmed the existence of one $-O^tBu$ end group with peaks at δ 28.05 and 65.83 ppm and one terminal hydroxybutyrate unit with signals at δ 21.80, 64.07, and 172.01 ppm. No signals assigned to the $-COOH$ group were observed in the NMR spectra (1H and $^{13}C\{^1H\}$), implying the absence of a OH-derived polymer. This is in agreement with the inability of $L-M-OH$ to initiate a polymeric chain, as shown in previous reports.^{7d} It should be noted that the PHB oligomer obtained using 3 has an identical 1H NMR spectrum with that obtained by using 3b (Figure S51). The multinuclear NMR analyses of the PLA oligomer obtained by using 3 also revealed the sole $-O^tBu$ end group in the PLA (Figure S50). The structures and end groups of the PHB oligomers obtained by complex 3b and mixture 3 were further investigated by the MALDI-TOF mass spectrometry, as shown Figures 5 and S52. The polymer chain was separated by the mass of a β -butyrolactone unit (86.03 amu), and monomodal molecular weight distributions were observed in both cases with many of peaks having same mass weight, indicating the sole $-O^tBu$ initiation group (73.06 amu) in both cases that was identical to the NMR analyses.

Then, a new question was raised based on the above observations regarding the exact structure of active species of 3b during the polymerization of *rac*-BBL: does it maintain the binuclear structure or decompose to a mononuclear active phosphasalalen- $Y-O^tBu$ (β -butyrolactone) and an inactive phosphasalalen- $Y-OH$ (β -butyrolactone)? As previous reported, the excess lactone monomers could easily decompose the binuclear catalytic precursors.^{7d} In our trials, when 2 equiv of *rac*-BBL was added to the solution of pure complex 3b, the signals in the $^{31}P\{^1H\}$ NMR spectrum shifted to the lower field (from δ 33.32 to 32.33 ppm) but retained a singlet peak, implying that the decomposition of 3b might not take place. The kinetic investigations of the *rac*-BBL polymerization were conducted by 3 and the binuclear complex 3b (Figure 9). For 3, the reaction kinetic featured a first-order dependence in the *rac*-BBL concentration (also on the catalyst concentration, see Figures S53–S54), and the semilogarithmic plot of $\ln([BBL]_0/[BBL]_t)$ vs time was linear with a slope of $k_{obs} = 7.00 \times 10^{-5} s^{-1}$, a value that is among those of the efficient catalysts for *rac*-BBL polymerization when compared to previous reports.^{7,17b} For complex 3b, however, a zero-order dependence on the *rac*-BBL concentration was adopted, and the slope of linear plot involving $[BBL]_0 - [BBL]_t$ vs time was $k_{obs} = 6.87 \times 10^{-5} s^{-1}$. The completely distinct reaction kinetic characteristics between the 3 and 3b demonstrated that the active species 3a (as the main component of 3) was structurally different compared to 3b in the catalytic systems for the polymerization of *rac*-BBL. Furthermore, the SEC curves obtained by 3 and 3b were monomodal; however, when the mixture of 3 and 3b (1:1) as catalysts was in the same proportion, the molecular weight distribution of the resultant polymer became wider, and a noticeable bimodal curve was observed (Figure 10). Based on all the above observations, it is reasonable to conclude that the binuclear structure of 3b was maintained during the polymerization (Scheme S1). The narrow molecular weight distribution of PHBs catalyzed by 3 was attributed to the low content of 3b and the probable presence of a transesterification side reaction in the polymerization of *rac*-BBL.

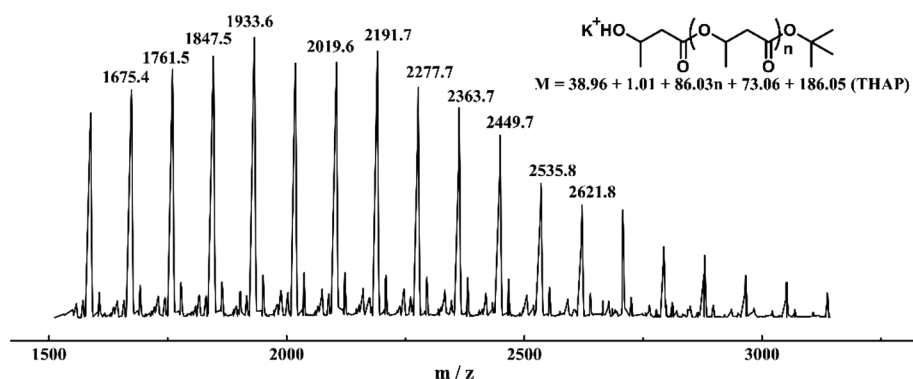


Figure 8. MALDI-TOF mass spectrum of the PHB oligomer prepared from complex **3b** ([BBL] = 2M, [I]:[BBL] = 1:20, toluene, and 25 °C).

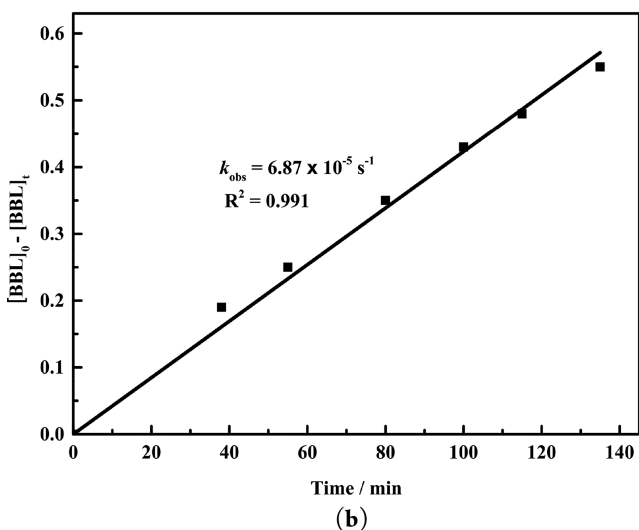
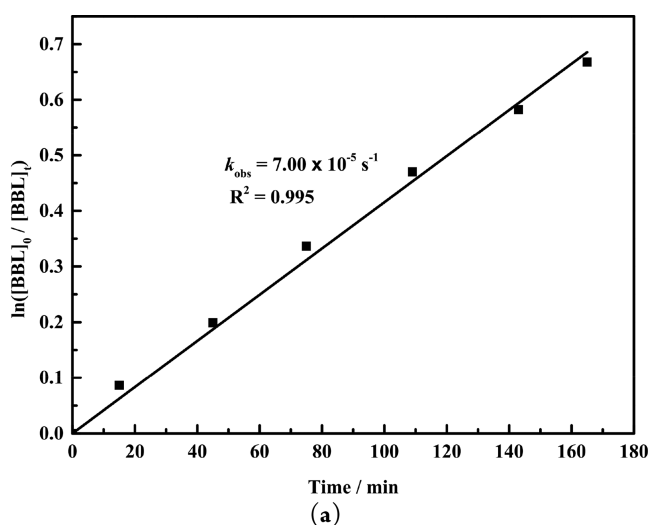


Figure 9. (a) Plot of $\ln([BBL]_0/[BBL]_t)$ vs time using **3** and (b) plot of $[BBL]_0 - [BBL]_t$ vs time using complex **3b** for the ROP of *rac*-BBL. Conditions are as follows: [BBL] = 2 M, [I]:[BBL] = 1:200, toluene, and 25 °C.

CONCLUSIONS

In conclusion, a family of rare-earth complexes bearing new phosphasalalen ligands, which were salen analogues with an iminophosphorane replacing the imine functionality, were synthesized and tested for the syndiotactic ROP of *rac*-LA and

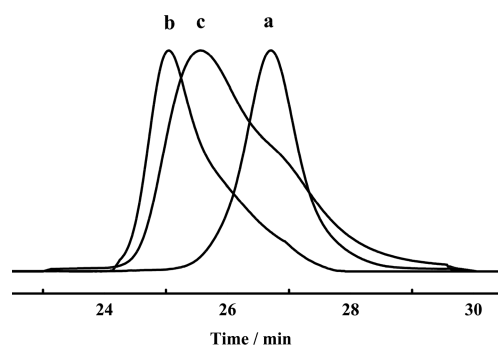


Figure 10. SEC curves of PHB polymers prepared from (a) **3**, (b) **3b**, and (c) 50% **3** + 50% **3b**. Conditions are as follows: [BBL] = 2 M, [BBL]:[I] = 200, toluene, and 25 °C.

rac-BBL. The new phosphasalalen pro-ligands **L1–L3** with chiral pyrrolidine backbones could be synthesized efficiently by the Kirsanov reaction between phosphinophenol and amino-pyrrolidinylphenols, and the multinuclear NMR and X-ray diffraction analyses revealed that their corresponding rare-earth mixtures **1–6** each contained a mononuclear complex and a binuclear complex with bridged alkoxy and hydroxy groups. However, when a trimethylsiloxide group was involved, the pure binuclear complex **7b** was formed. All the complexes could catalyze the heteroselective ROP of *rac*-BBL to produce syndiotactic polymers (P_r up to 0.73). The high polymerization activities of **2–6** in *rac*-BBL ROP could be rationalized by the better electron-donating ability of the chelating phosphasalalen ligands compared to their salen analogues. Not surprisingly, **1** with a more Lewis acidic scandium center was inactive. The detailed end-group analyses and the kinetic investigations proved the absence of hydroxy-derived PHBs and, interestingly, that the binuclear structures of the alkoxy–hydroxy-bridged complexes did not decompose during the polymerization.

EXPERIMENTAL SECTION

General Considerations. All reactions were conducted under an atmosphere of dry nitrogen using standard Schlenk line and glovebox (Vigor SG1200/750TS-F) techniques. Solvents and reagents were obtained from commercial sources. THF, toluene, and hexane were distilled from sodium or benzophenone, and DCM was distilled from CaH_2 . Commercial reagents, namely $^n\text{BuLi}$, *N*-bromosuccinimide, chlorodiphenylphosphine, and other commercially available reagents,

were purchased from TCI or Aladdin and used without further purification. *rac*-Lactide was recrystallized from ethyl acetate and sublimated twice. The phosphinophenols and aminopyrrolidinylphenols with bulky substituents at the *ortho*-phenoxide positions were prepared according to the methods reported in previous literature.⁸ ¹H (400 MHz), ³¹P{¹H} (162 MHz), and ¹³C{¹H} NMR (100 MHz) and ¹H DOSY (600 MHz) measurements were obtained on a JNM-ECZ400S/L 400 or Bruker AV600 MR spectrometer, respectively, in a CDCl₃, THF-*d*₆, or C₆D₆ solution (25 °C). The molecular weights and molecular weight distribution of the polymers were measured by means of gel-permeation chromatography (SEC) on a Waters LC-16 (35 °C) instrument. The *M_n* values of the PLAs were corrected with a 0.58 factor, and those of the PHBs were not corrected. Single crystals suitable for X-ray analysis were obtained from *n*-hexane solutions. The intensity data of the single crystals were collected on the Bruker D8 Venture system. All determinations of the unit cell and intensity data were performed with graphite-monochromated Ga K α radiation (λ = 1.34138 Å). The data of the complexes were collected at 173 k using the ω -scan technique. All the non-hydrogen atoms were refined anisotropically, and all the hydrogen atoms were included but not refined. Crystallographic data (excluding structure factors, Table S2) for the structure analysis were deposited with the Cambridge Crystallographic Data Centre as CCDC 2031008 (3b), 2031009 (6b), and 2031010 (7b).

Synthesis of Pro-Ligand L1. At -78 °C, bromine (6.1 mmol) was added dropwise to a solution of 2,4-di-*tert*-butyl-6-(diphenylphosphanyl)phenol (2.3 g, 6.0 mmol) in dry dichloromethane (20 mL). The solution was still stirred at -78 °C for 1 h. DABCO (3.6 mmol) and (S)-2-((2-(aminomethyl)pyrrolidin-1-yl)methyl)-4,6-di-*tert*-butylphenol (2.4 g, 6.1 mmol) were dissolved in DCM and added to the solution dropwise. The solution was stirring at -78 °C for another 4 h, then warmed to room temperature and stirred overnight. The cloudy solution was quenched and washed with water (2 × 100 mL). The organic solution was dried over anhydrous Na₂SO₄ and evaporated in a vacuum. After recrystallization from Et₂O, the pure product was isolated as a white solid (2.4 g, 50.8%). ¹H NMR (400 MHz, CDCl₃, ppm): δ 7.86–6.58 (m, 14H, Ph-H), 4.80 (d, 1H, NH-CH₂), 4.59 (m, 1H, N-CH₂-Ph), 3.95 (d, 1H, NH-CH₂), 3.85 (m, 1H, N-CH₂-Ph), 3.20 (m, 1H, N-CH), 2.95 (m, 2H, N-CH₂-CH₂), 2.30 (m, 1H, N-CH₂-CH₂), 1.89 (m, 1H, N-CH₂-CH₂), 1.62 (m, 2H, N-CH-CH₂), 1.26 (s, 9H, C(CH₃)₃), 1.17 (s, 9H, C(CH₃)₃), 1.14 (s, 9H, C(CH₃)₃), 1.02 (s, 9H, C(CH₃)₃). ³¹P{¹H} NMR (162 MHz, CDCl₃, ppm): δ 44.87 (s, P). ¹³C{¹H} NMR (100 MHz, CDCl₃, ppm): δ 167.95, 153.49, 141.69, 141.54, 139.07, 137.82, 137.64, 133.33, 133.21, 132.96, 132.86, 131.18, 131.92, 131.81, 129.61, 129.47, 129.30, 129.18, 129.13, 128.92, 128.12, 127.82, 127.16, 125.81, 125.37, 119.58, 68.29 (s, N-CH-CH₂-N), 68.23 (s, N-CH-CH₂-N), 59.54 (s, N-CH₂-Ph), 53.39 (s, N-CH), 47.58 (s, N-CH₂), 35.35 (s, Ph-C-CH₃), 35.34 (s, Ph-C-CH₃), 35.10 (s, Ph-C-CH₃), 34.12 (s, Ph-C-CH₃), 31.62 (s, N-CH-CH₂), 31.26 (s, C-CH₃), 30.01 (s, N-CH₂-CH₂), 29.92 (s, C-CH₃), 28.61 (s, C-CH₃), 23.32 (s, C-CH₃). Anal. Calc. for C₄₆H₆₄BrN₂O₂P: C, 70.12; H, 8.19; N, 3.56. Found: C, 70.18; H, 8.14; N, 3.58.

Synthesis of Pro-Ligand L2. The synthesis of pro-ligand L2 was carried out in the same way as that described for pro-ligand L1, but 2-adamantanyl-6-(diphenylphosphanyl)-4-methylphenol (2.6 g, 6 mmol) and 2-adamantanyl-6-(((S)-2-(aminomethyl)pyrrolidin-1-yl)methyl)-4-methylphenol (2.2 g, 6.1 mmol) were used. The pure product was obtained by column chromatography on silica gel (DCM/MeOH 30:1) as a yellow solid (2.5 g, 48.9%). ¹H NMR (400 MHz, CDCl₃, ppm): δ 7.88–6.11 (m, 14H, Ph-H), 4.80 (m, 1H, NH-CH₂), 4.56 (m, 1H, N-CH₂-Ph), 4.01 (d, 1H, NH-CH₂), 3.87 (m, 1H, N-CH₂-Ph), 3.14 (m, 1H, N-CH), 2.97 (m, 2H, N-CH₂), 2.11 (s, 3H, Ph-CH₃), 2.03 (s, 3H, Ph-CH₃), 1.99–1.65 (m, 30H, Ph-Ad(H) and pyrrolidine-ring(H)), 1.51 (m, 2H, Ph-Ad(H)), 1.42 (m, 2H, Ph-Ad(H)). ³¹P{¹H} NMR (162 MHz, CDCl₃, ppm): δ 44.46 (s, P). ¹³C{¹H} NMR (100 MHz, CDCl₃, ppm): δ 168.89, 153.77, 142.01, 141.93, 140.11, 135.83, 133.30, 133.29, 133.00, 132.90, 132.44, 132.31, 131.75, 131.64, 131.19,

129.64, 129.50, 129.44, 129.31, 129.22, 129.11, 128.52, 128.30, 127.31, 126.05, 124.93, 123.90, 120.10, 102.63, 101.53, 68.19 (s, N-CH-CH₂-N), 68.13 (s, N-CH-CH₂-N), 65.94 (s, N-CH₂-Ph), 59.26 (s, N-CH), 53.71 (s, N-CH₂), 47.50 (s, Ph-Ad(C)), 40.27 (s, Ph-Ad(C)), 40.22 (s, Ph-Ad(C)), 37.16 (s, Ph-Ad(C)), 36.97 (s, Ph-CH₃), 36.85 (s, Ph-CH₃), 29.23 (s, Ph-Ad(C)), 28.85 (s, N-CH₂-CH₂), 28.51 (s, Ph-Ad(C)), 23.22 (s, Ph-Ad(C)), 20.87 (s, Ph-Ad(C)). Anal. Calc. for C₅₂H₆₄BrN₂O₂P: C, 72.63; H, 7.50; N, 3.26. Found: C, 72.86; H, 7.64; N, 3.30.

Synthesis of Pro-Ligand L3. The synthesis of pro-ligand L3 was carried out in the same way as that described for pro-ligand L1, but 2-(diphenylphosphanyl)-4-methyl-6-(2-phenylpropan-2-yl)phenol (2.5 g, 6 mmol) and (S)-2-((2-(aminomethyl)pyrrolidin-1-yl)methyl)-4-methyl-6-(2-phenylpropan-2-yl)phenol (2.1 g, 6.1 mmol) were used. The pure product was obtained by column chromatography on silica gel (DCM/MeOH 30:1) as a yellow solid (2.3 g, 47.3%). ¹H NMR (400 MHz, CDCl₃, ppm): δ 7.92–6.11 (m, 24H, Ph-H), 4.06 (d, 1H, N-CH₂-Ph), 3.86 (d, 1H, NH-CH₂), 3.83 (d, 1H, NH-CH₂), 3.59 (m, 1H, N-CH₂-Ph), 2.92 (m, 1H, N-CH-CH₂), 2.33 (dd, 1H, N-CH₂), 2.13 (s, 3H, Ph-CH₃), 2.08 (s, 3H, Ph-CH₃), 2.06 (m, 1H, N-CH₂-CH₂), 1.72 (s, 3H, C-CH₃), 1.62 (s, 3H, C-CH₃), 1.60 (s, 3H, C-CH₃), 1.45 (s, 3H, C-CH₃). ³¹P{¹H} NMR (162 MHz, CDCl₃, ppm): δ 42.67 (s, P). ¹³C{¹H} NMR (100 MHz, CDCl₃, ppm): δ 169.68, 152.07, 150.58, 149.43, 148.67, 147.93, 140.56, 140.48, 136.64, 135.67, 135.46, 133.15, 133.05, 132.43, 131.97, 130.76, 130.41, 129.25, 129.12, 129.01, 128.42, 127.89, 127.29, 126.80, 126.40, 125.99, 125.88, 125.46, 124.53, 121.32, 120.26, 68.20 (s, NH-CH₂), 55.38 (s, N-CH₂-Ph), 50.71 (s, N-CH-CH₂-N), 46.41 (s, NH-CH₂), 42.48 (s, Ph-C-Ph), 41.84 (s, N-C-CH₂), 30.16 (s, N-CH-CH₂-CH₂), 29.54 (s, Ph-CH₃), 29.39 (s, C-CH₃), 28.95 (s, N-CH₂-CH₂), 25.80 (s, C-CH₃), 21.01 (s, C-CH₃), 20.93 (s, C-CH₃). Anal. Calc. for C₅₀H₅₆BrN₂O₂P: C, 72.54; H, 6.82; N, 3.38. Found: C, 72.98; H, 6.69; N, 3.39.

Synthesis of Mixture 1. In the glovebox, NaHMDS (55.1 mg, 0.3 mmol) was added to a solution of pro-ligand L1 (78.8 mg, 0.1 mmol) in THF (6 mL) under continuous stirring at -30 °C. Then, the solution was warmed to room temperature and left stirring for 4 h. The insoluble sodium bromide byproduct was removed from the solution by centrifugation before the subsequent addition of a cooled THF solution of ScCl₃(THF)₃ (151.3 mg, 0.10 mmol) at -30 °C. After stirring for 4 h at RT, lots of white solids were formed and again removed by centrifugation to give a light yellow transparent solution. ^tBuOK (11.2 mg, 0.10 mmol) was then added to the reaction mixture, and a white slurry was immediately formed. The cloudy solution was stirred for another 2 h at 50 °C and centrifuged to remove all remaining insoluble salts, and the filtrate was evaporated to dryness and washed with cold hexane. Crystallization in hexane at -30 °C gave the mixture 1 as a white solid in a 49.8% yield (44.8 mg). ¹H NMR (400 MHz, C₆D₆, ppm): δ 7.67–6.60 (m, 14H, Ph-H), 4.00 (m, 1H, P=N-CH₂), 3.52 (m, 1H, P=N-CH₂; 1H, N-CH₂-Ph), 3.10 (m, 1H, N-CH₂-Ph), 3.00 (m, 1H, N-CH), 2.74 (m, 1H, N-CH₂), 2.56 (m, 1H, N-CH₂), 2.15 (m, 2H, N-CH₂-CH₂; 1H, N-CH-CH₂), 1.91 (m, 1H, N-CH-CH₂), 1.85 (s, 9H, C(CH₃)₃), 1.84 (s, 9H, O-C(CH₃)₃), 1.43 (s, 9H, C(CH₃)₃), 1.19 (s, 9H, C(CH₃)₃), 1.10 (s, 9H, C(CH₃)₃). ³¹P{¹H} NMR (162 MHz, C₆D₆, ppm): δ 37.15 (s, P), 34.97 (s, P). Due to the asymmetric inheritance of both mononuclear and binuclear components (the presence of a chiral carbon) in the mixture, we could not unambiguously assign the ¹³C{¹H} NMR signals. ¹³C{¹H} NMR (100 MHz, C₆D₆, ppm): δ 167.02, 160.77, 136.05, 135.38, 135.24, 134.15, 133.91, 132.56, 132.47, 132.23, 132.15, 131.55, 131.45, 130.77, 129.40, 129.12, 127.62, 127.42, 125.81, 125.68, 124.01, 123.81, 123.25, 122.84, 111.66, 110.44, 69.64, 68.05, 66.57, 58.36, 51.55, 34.94, 34.89, 34.71, 34.70, 34.42, 34.33, 32.99, 32.95, 32.88, 31.02, 30.67, 30.32, 30.21, 28.93, 26.60, 24.51, 21.76, 19.36.

Synthesis of Mixture 2. The mixture 2 was synthesized using the same procedure as that for complex 1, but pro-ligand L1 (78.8 mg, 0.10 mmol), YCl₃(THF)_{3.5} (44.8 mg, 0.10 mmol), and KOEt (8.6 mg, 0.10 mmol) were used. Mixture 2 was obtained in a 49.4% yield as a

white solid (45.4 mg). ^1H NMR (400 MHz, C_6D_6 , ppm): δ 7.72–6.41 (m, 14H, Ph–H), 4.75 (d, 1H, P=N–CH₂), 4.57 (d, 1H, P=N–CH₂), 3.25–3.75 (m, 2H, N–CH₂–Ph; 2H, O–CH₂; 1H, N–CH), 3.08 (m, 1H, N–CH₂), 2.84 (m, 1H, N–CH₂), 1.89 (s, 9H, C(CH₃)₃), 1.51 (s, 9H, C(CH₃)₃), 1.46 (s, 9H, C(CH₃)₃), 1.35 (d, 3H, O–CH₂–CH₃), 1.13 (s, 9H, C(CH₃)₃). $^{31}\text{P}\{^1\text{H}\}$ NMR (162 MHz, C_6D_6 , ppm): δ 36.72 (s, P), 33.05 (s, P). Due to the asymmetric inheritance of both mononuclear and binuclear components (the presence of a chiral carbon) in the mixture, we could not unambiguously assign the $^{13}\text{C}\{^1\text{H}\}$ NMR signals. $^{13}\text{C}\{^1\text{H}\}$ NMR (100 MHz, C_6D_6 , ppm): δ 167.63, 162.54, 139.00, 136.54, 135.50, 134.43, 133.64, 133.56, 132.16, 132.07, 131.50, 130.75, 129.02, 128.61, 128.42, 128.31, 128.21, 127.27, 127.08, 125.38, 125.21, 123.78, 123.67, 112.82, 110.65, 59.92, 58.69, 51.56, 51.11, 35.97, 35.32, 35.23, 33.88, 33.83, 33.79, 32.09, 31.98, 31.40, 31.28, 30.75, 29.86, 29.65, 23.96, 21.84, 20.76.

Synthesis of Mixture 3. The mixture 3 was synthesized using the same procedure as that for mixture 1, but pro-ligand L1 (78.8 mg, 0.10 mmol), $\text{YCl}_3(\text{THF})_{3.5}$ (44.7 mg, 0.10 mmol), and KO^tBu (11.2 mg, 0.10 mmol) were used. The mixture 3 was obtained in a 51.2% yield as a white solid (48.5 mg). The crystal of complex 3b was slowly grown from the concentrated solution of mixture 3 in hexane. ^1H NMR (400 MHz, C_6D_6 , ppm): δ 7.73–6.62 (m, 14H, Ph–H), 4.01 (m, 1H, P=N–CH₂), 3.59 (br, 1H, N–CH₂–Ph), 3.14 (t, 1H, P=N–CH₂), 3.06 (br, 1H, N–CH₂–Ph), 2.76 (m, 1H, N–CH), 2.67 (t, 1H, N–CH₂), 2.20 (m, 1H, N–CH₂), 2.09 (m, 2H, N–CH–CH₂), 1.89 (m, 1H, N–CH₂–CH₂), 1.83 (m, 1H, N–CH₂–CH₂), 1.81 (s, 9H, C(CH₃)₃), 1.49 (s, 9H, O–C(CH₃)₃), 1.25 (s, 9H, C(CH₃)₃), 1.19 (s, 9H, C(CH₃)₃), 1.13 (s, 9H, C(CH₃)₃). $^{31}\text{P}\{^1\text{H}\}$ NMR (162 MHz, C_6D_6 , ppm): δ 36.94 (s, P), 33.32 (s, P). Due to the asymmetric inheritance of both mononuclear and binuclear components (the presence of a chiral carbon) in the mixture, we could not unambiguously assign the $^{13}\text{C}\{^1\text{H}\}$ NMR signals. $^{13}\text{C}\{^1\text{H}\}$ NMR (100 MHz, C_6D_6 , ppm): δ 167.36, 161.41, 139.75, 139.68, 136.48, 136.01, 135.87, 135.60, 133.53, 133.44, 132.59, 132.49, 131.62, 129.01, 128.58, 128.47, 128.45, 128.36, 127.02, 126.89, 124.99, 124.30, 123.70, 113.19, 112.01, 70.21, 69.02, 68.84, 67.94, 59.44, 52.25, 48.77, 35.90, 35.62, 35.36, 34.31, 33.96, 32.10, 31.94, 31.43, 31.29, 30.98, 30.07, 30.03, 27.22, 25.42, 20.65.

3b ^1H NMR (400 MHz, C_6D_6 , ppm): δ 7.73–6.50 (m, 14H, Ph–H), 4.65 (d, 1H, P=N–CH₂), 3.48 (m, 1H, N–CH₂–Ph), 3.32 (d, 1H, P=N–CH₂), 3.26 (m, 1H, N–CH₂–Ph), 2.72 (dt, 2H, N–CH), 1.89 (s, 9H, C(CH₃)₃), 1.87 (s, 4.5H, O–C(CH₃)₃), 1.76 (m, 2H, N–CH₂–CH₂, 2H, N–CH–CH₂), 1.66 (s, 9H, C(CH₃)₃), 1.39 (s, 9H, C(CH₃)₃), 1.14 (s, 9H, C(CH₃)₃). $^{31}\text{P}\{^1\text{H}\}$ NMR (162 MHz, C_6D_6 , ppm): δ 33.32 (s, P). $^{13}\text{C}\{^1\text{H}\}$ NMR (100 MHz, C_6D_6 , ppm): δ 167.25, 161.61, 139.79, 139.05, 136.51, 135.28, 135.13, 134.86, 133.44, 133.29, 132.04, 131.95, 131.44, 130.68, 128.78, 128.58, 128.48, 125.06, 124.32, 123.69, 112.55, 112.09, 111.32, 70.73 (s, P=N–CH₂), 67.78 (s, NH–CH₂), 64.50 (s, N–CH₂–Ph), 59.44 (s, O–C–CH₃), 52.23 (s, N–CH), 51.68 (s, N–CH₂), 35.85 (s, C–CH₃), 35.67 (s, C–CH₃), 35.29 (s, C–CH₃), 33.87 (s, N–CH–CH₂), 33.80 (s, N–CH₂–CH₂), 32.00 (s, C–CH₃), 31.32 (s, C–CH₃), 31.00 (s, C–CH₃), 30.04 (s, C–CH₃), 27.33 (s, C–CH₃), 25.35 (s, C–CH₃), 24.47 (s, C–CH₃), 22.74 (s, C–CH₃), 21.28 (s, C–CH₃), 20.54 (s, C–CH₃). Anal. Calc. for $\text{C}_{96}\text{H}_{132}\text{N}_4\text{O}_6\text{P}_2\text{Y}_2$: C, 68.72; H, 7.93; N, 3.34. Found: C, 69.32; H, 8.23; N, 3.26.

Synthesis of Mixture 4. The mixture 4 was synthesized using the same procedure as that for mixture 1, but pro-ligand L1 (78.8 mg, 0.10 mmol), $\text{LuCl}_3(\text{THF})_3$ (49.8 mg, 0.10 mmol), and KO^tBu (11.2 mg, 0.10 mmol) were used. The mixture 5 was obtained in a 45.5% yield as a white solid (47.4 mg). ^1H NMR (400 MHz, C_6D_6 , ppm): δ 7.85–6.72 (m, 14H, Ph–H), 4.16 (d, 1H, P=N–CH₂), 3.21 (m, 1H, N–CH₂–Ph), 3.12 (m, 1H, N–CH₂–Ph), 2.90 (m, 1H, N–CH), 2.63 (d, 1H, P=N–CH₂), 2.23 (m, 2H, N–CH₂; 2H, N–CH–CH₂), 1.98 (m, 2H, N–CH₂–CH₂), 1.95 (s, 9H, C(CH₃)₃), 1.69 (s, 9H, O–C(CH₃)₃), 1.38 (s, 9H, C(CH₃)₃), 1.28 (s, 9H, C(CH₃)₃), 1.18 (s, 9H, C(CH₃)₃). $^{31}\text{P}\{^1\text{H}\}$ NMR (162 MHz, C_6D_6 , ppm): δ 38.94 (s, P), 34.31 (s, P). Due to the asymmetric inheritance of both

mononuclear and binuclear components (the presence of a chiral carbon) in the mixture, we could not unambiguously assign the $^{13}\text{C}\{^1\text{H}\}$ NMR signals. $^{13}\text{C}\{^1\text{H}\}$ NMR (100 MHz, C_6D_6 , ppm): δ 167.99, 161.73, 140.20, 140.12, 137.02, 136.38, 136.24, 135.95, 133.54, 133.45, 132.51, 132.42, 131.76, 131.28, 130.36, 129.21, 128.81, 128.61, 128.50, 128.41, 124.78, 124.24, 123.82, 112.60, 111.44, 71.08, 69.26, 69.09, 59.13, 52.52, 48.50, 48.46, 35.69, 35.41, 34.20, 33.98, 33.93, 32.09, 32.01, 31.66, 31.40, 31.30, 30.15, 27.63, 20.31.

Synthesis of Mixture 5. The mixture 5 was synthesized using the same procedure as that for mixture 1, but pro-ligand L2 (87.6 mg, 0.10 mmol), $\text{YCl}_3(\text{THF})_{3.5}$ (44.8 mg, 0.10 mmol), and KOEt (8.6 mg, 0.10 mmol) were used. The mixture 5 was obtained in a 43.4% yield as a yellow solid (59.7 mg). ^1H NMR (400 MHz, C_6D_6 , ppm): δ 7.55–6.41 (m, 14H, Ph–H), 4.67 (d, 1H, P=N–CH₂), 3.35 (m, 2H, N–CH₂–Ph; 1H, N–CH), 2.91 (m, 2H, O–CH₂–CH₃), 2.69 (d, 1H, P=N–CH₂), 2.56 (m, 2H, N–CH₂), 2.45 (m, 10H, Ph–Ad(H)), 2.35 (d, 3H, Ph–CH₃), 2.13 (d, 3H, O–CH₂–CH₃), 2.06 (s, 3H, Ph–CH₃), 2.06–1.64 (m, 20H, Ph–Ad(H)). $^{31}\text{P}\{^1\text{H}\}$ NMR (162 MHz, CDCl_3 , ppm): δ 35.62 (s, P), 32.28 (s, P). Due to the asymmetric inheritance of both mononuclear and binuclear components (the presence of a chiral carbon) in the mixture, we could not unambiguously assign the $^{13}\text{C}\{^1\text{H}\}$ NMR signals. $^{13}\text{C}\{^1\text{H}\}$ NMR (100 MHz, C_6D_6 , ppm): δ 167.96, 162.87, 139.86, 137.97, 137.26, 136.68, 135.80, 134.57, 133.85, 132.66, 132.05, 131.38, 131.12, 129.42, 129.30, 129.19, 128.89, 128.66, 125.79, 124.76, 122.60, 122.44, 121.98, 115.94, 114.70, 63.77, 63.56, 61.25, 59.35, 59.22, 53.11, 52.67, 52.35, 41.34, 41.14, 38.24, 38.14, 37.91, 37.78, 37.69, 37.62, 37.54, 30.32, 30.21, 30.12, 30.05, 29.85, 25.04, 21.62, 21.55, 21.43, 21.16.

Synthesis of Mixture 6. The mixture 6 was synthesized using the same procedure as that for mixture 1, but pro-ligand L3 (82.8 mg, 0.10 mmol), $\text{YCl}_3(\text{THF})_{3.5}$ (44.8 mg, 0.10 mmol), and KOEt (8.6 mg, 0.10 mmol) were used. The mixture 6 was obtained in a 41.4% yield as a pale yellow solid (50.7 mg). The crystal of 6b was slowly grown from the concentrated solution of mixture 6 in hexane. ^1H NMR (400 MHz, C_6D_6 , ppm): δ 7.53–6.54 (m, 24H, Ph–H), 3.79 (d, 2H, P=N–CH₂), 3.24 (m, 2H, O–CH₂–CH₃), 2.54–2.72 (m, 2H, N–CH₂–Ph; 1H, N–CH; 2H, N–CH₂), 2.31 (s, 3H, Ph–CH₃), 2.28 (s, 1H, N–CH–CH₂), 2.26 (s, 1H, N–CH–CH₂), 2.22 (d, 3H, Ph–CH₃), 2.18 (m, 1H, N–CH₂–CH₂), 2.14 (d, 1H, N–CH₂–CH₂), 1.98 (s, 3H, C–CH₃), 1.88 (s, 3H, C–CH₃), 1.83 (s, 3H, C–CH₃), 1.80 (s, 3H, C–CH₃). $^{31}\text{P}\{^1\text{H}\}$ NMR (162 MHz, C_6D_6 , ppm): δ 34.94 (s, P), 31.29 (s, P). Due to the asymmetric inheritance of both mononuclear and binuclear components (the presence of a chiral carbon) in the mixture, we could not unambiguously assign the $^{13}\text{C}\{^1\text{H}\}$ NMR signals. $^{13}\text{C}\{^1\text{H}\}$ NMR (100 MHz, C_6D_6 , ppm): δ 167.84, 162.17, 153.07, 152.61, 139.16, 137.01, 134.46, 133.58, 132.55, 131.98, 131.44, 130.28, 129.59, 129.12, 127.82, 127.48, 127.31, 126.78, 125.96, 125.77, 125.53, 125.28, 122.95, 122.60, 121.98, 115.59, 114.3, 64.97, 59.55, 59.21, 53.35, 52.45, 51.75, 44.76, 43.90, 43.31, 43.05, 38.52, 33.72, 32.88, 31.02, 30.48, 28.84, 27.85, 24.84, 22.33, 21.60.

6b ^1H NMR (400 MHz, C_6D_6 , ppm): δ 7.45–6.35 (m, 24H, Ph–H), 3.95 (m, 2H, P=N–CH₂), 3.25 (m, 2H, O–CH₂–CH₃), 2.55–2.68 (m, 1H, N–CH₂–Ph; 2H, N–CH₂; 1H, N–CH), 2.37 (d, 1H, N–CH₂–Ph), 2.27 (s, 3H, Ph–CH₃), 2.24 (d, 1H, N–CH–CH₂), 2.15 (d, 1H, N–CH–CH₂), 2.09 (d, 2H, N–CH₂–CH₂), 2.02 (s, 3H, Ph–CH₃), 1.94 (s, 3H, C–CH₃), 1.84 (s, 3H, C–CH₃), 1.79 (s, 3H, C–CH₃), 1.76 (s, 3H, C–CH₃). $^{31}\text{P}\{^1\text{H}\}$ NMR (162 MHz, C_6D_6 , ppm): δ 31.29 (s, P). $^{13}\text{C}\{^1\text{H}\}$ NMR (100 MHz, C_6D_6 , ppm): δ 170.21, 164.82, 156.60, 155.45, 154.15, 153.26, 139.34, 138.54, 135.27, 133.30, 133.25, 131.70, 131.45, 131.22, 130.62, 130.15, 127.04, 126.86, 126.62, 125.60, 125.17, 124.98, 123.98, 123.66, 123.51, 116.66, 116.28, 69.10 (s, O–C–CH₂), 57.42 (s, P=N–CH₂), 54.36 (s, N–CH₂–Ph), 53.65 (s, N–CH–CH₂), 44.93 (s, N–CH₂), 42.30 (s, N–CH₂), 33.61 (s, Ph–C–CH₃), 31.66 (s, Ph–C–CH₃), 30.62 (s, Ph–C–CH₃), 30.10 (s, Ph–C–CH₃), 28.51 (s, N–CH–CH₂), 27.21 (s, Ph–CH₃), 25.61 (s, C–CH₃), 22.75 (s, Ph–CH₃), 20.94 (s, C–CH₃). Anal. Calc. for $\text{C}_{102}\text{H}_{112}\text{N}_4\text{O}_6\text{P}_2\text{Y}_2$: C, 70.82; H, 6.53; N, 3.24. Found: C, 71.69; H, 6.61; N, 3.17.

Synthesis of Complex 7b. The complex **7b** was synthesized using the same procedure as that for mixture **1**, but pro-ligand **L1** (78.8 mg, 0.10 mmol), $\text{YCl}_3(\text{THF})_{3.5}$ (44.8 mg, 0.10 mmol), and KOSiMe_3 (13.0 mg, 0.10 mmol) were used. The complex **7b** was obtained in a 49.8% yield as a pale yellow solid (42.2 mg, 0.025 mmol). The crystal of **7b** was slowly grown from the concentrated solution of hexane. ^1H NMR (400 MHz, C_6D_6 , ppm): δ 7.66–6.44 (m, 14H, Ph–H), 4.55 (d, 1H, P=N–CH₂), 3.38 (m, 1H, N–CH₂–Ph), 3.28 (d, 1H, P=N–CH₂), 3.23 (m, 1H, N–CH₂–Ph), 2.68 (m, 1H, N–CH₂; 2H, N–CH₂), 1.83 (s, 9H, C(CH₃)₃), 1.74 (m, 2H, N–CH–CH₂), 1.64 (m, 1H, N–CH₂–CH₂), 1.61 (s, 9H, C(CH₃)₃), 1.35 (m, 1H, N–CH₂–CH₂), 1.31 (s, 9H, C(CH₃)₃), 1.07 (s, 9H, C(CH₃)₃), 0.59 (s, 4.5H, Si–(CH₃)₃). $^{31}\text{P}\{^1\text{H}\}$ NMR (162 MHz, C_6D_6 , ppm): δ 33.13 (s, P). $^{13}\text{C}\{^1\text{H}\}$ NMR (100 MHz, C_6D_6 , ppm): δ 167.02, 161.57, 139.14, 139.06, 136.52, 135.58, 135.43, 135.04, 134.69, 133.31, 133.22, 132.10, 132.00, 131.44, 130.67, 128.86, 128.63, 128.31, 128.91, 125.06, 123.97, 123.87, 112.79, 111.51, 64.28 (s, P=N–CH₂–CH), 64.09 (s, N–CH₂–Ph), 59.27 (s, N–CH), 51.84 (s, N–CH₂), 35.91 (s, Ph–C–CH₃), 35.90 (s, Ph–C–CH₃), 35.25 (s, Ph–C–CH₃), 31.98 (s, N–CH–CH₂), 31.65 (s, Ph–C–CH₃), 31.43 (s, N–CH₂–CH₂), 31.31 (s, C–CH₃), 31.17 (s, C–CH₃), 30.17 (s, C–CH₃), 29.91 (s, C–CH₃), 24.55 (s, C–CH₃), 22.74 (s, C–CH₃), 21.29 (s, C–CH₃). Anal. Calc. for $\text{C}_{95}\text{H}_{132}\text{N}_4\text{O}_6\text{P}_2\text{SiY}_2$: C, 67.36; H, 7.85; N, 3.31. Found: C, 67.93; H, 7.64; N, 3.34.

General Polymerization of *rac*-Lactide. In a glovebox, *rac*-LA (288 mg, 2 mmol, 200 equiv) was dissolved in THF (1 mL). A solution of the catalyst (10 μmol in 1 mL THF) was injected into the reaction mixture (5 μmol catalyst was used when $[\text{LA}]/[\text{I}] \geq 500$) such that the overall concentration of *rac*-LA was 1 M. Aliquots were taken from the reaction under a nitrogen atmosphere, quenched with hexane, and poured into hexane to precipitate the polymer. The polymer was then dried under a vacuum to a constant weight at 40 °C. Samples were analyzed by ^1H NMR spectroscopy to determine the conversion by the relative integration of signals at 5.06 (monomer) and 5.20 ppm (polymer). The P_r value was determined by integrating the methane region of the homonuclear decoupled ^1H NMR spectrum (δ 5.06–5.24 ppm). The number-averaged molecular weight and M_w/M_n of PLA were determined using gel-permeation chromatography (SEC).

As with **3** for example, the mole ratio of **3a**:**3b** in the mixture was 10:1 as indicated by $^{31}\text{P}\{^1\text{H}\}$ NMR spectrum. The relative molecular weight of 940.72 (867.00 (molecular weight of **3a**) \times 10/11 + 1677.89 (molecular weight of **3b**) \times 1/11 = 940.72) was used to calculate the scale of **3** for the polymerization of *rac*-LA and *rac*-BBL.

General Polymerization of *rac*-BBL. In the glovebox, a Schlenk flask was charged with a solution of the catalyst (10 mmol) in toluene (1 mL). To this solution was rapidly added *rac*-BBL (172.2 mg, 2 mmol, 200 equiv). The mixture was immediately stirred with a magnetic stir bar. After the scheduled time, the reaction was quenched with acidic methanol, and the polymer was precipitated with excess methanol. The conversion was monitored by comparing the relative magnitude of peaks corresponding to the methine hydrogen for *rac*-BBL and PHB. The polymer was then dried under vacuum to a constant weight at 40 °C. The P_r value was determined by integrating the methane region of the ^{13}C NMR spectrum (δ 169.34–169.21 ppm).

ASSOCIATED CONTENT

Supporting Information

The Supporting Information is available free of charge at <https://pubs.acs.org/doi/10.1021/acs.inorgchem.0c02741>.

^1H , $^{13}\text{C}\{^1\text{H}\}$, and $^{31}\text{P}\{^1\text{H}\}$ NMR spectra of pro-ligands and complexes (PDF)

Accession Codes

CCDC 2031008–2031010 contain the supplementary crystallographic data for this paper. These data can be obtained free of charge via www.ccdc.cam.ac.uk/data_request/cif, or by

emailing data_request@ccdc.cam.ac.uk, or by contacting The Cambridge Crystallographic Data Centre, 12 Union Road, Cambridge CB2 1EZ, UK; fax: +44 1223 336033.

AUTHOR INFORMATION

Corresponding Author

Xiaochao Shi – Department of Polymer Materials, College of Materials Science and Engineering, Shanghai University, Shanghai 200444, China; orcid.org/0000-0001-5178-7972; Email: xcshi@shu.edu.cn

Author

Hui Liu – Department of Polymer Materials, College of Materials Science and Engineering, Shanghai University, Shanghai 200444, China

Complete contact information is available at:

<https://pubs.acs.org/10.1021/acs.inorgchem.0c02741>

Notes

The authors declare no competing financial interest.

ACKNOWLEDGMENTS

This work was supported by the National Natural Science Foundation of China (no. 21704060) and the Program for Professor of Special Appointment (Eastern Scholar) at Shanghai Institutions of Higher Learning.

REFERENCES

- (1) (a) Mecking, S. Nature or Petrochemistry?—biologically degradable materials. *Angew. Chem., Int. Ed.* **2004**, *43*, 1078–1085. (b) Williams, C. K.; Hillmyer, M. A. Polymers from renewable resources: a perspective for a special issue of polymer reviews. *Polym. Rev.* **2008**, *48*, 1–10. (c) Platel, R. H.; Hodgson, L. M.; Williams, C. K. Biocompatible initiators for lactide polymerization. *Polym. Rev.* **2008**, *48*, 11–63. (d) Miller, S. A. Sustainable polymers: opportunities for the next decade. *ACS Macro Lett.* **2013**, *2*, 550–554. (e) Schröder, K.; Matyjaszewski, K.; Noonan, K. J.; Mathers, R. T. Towards sustainable polymer chemistry with homogeneous metal-based catalysts. *Green Chem.* **2014**, *16*, 1673–1686.
- (2) (a) Philip, S.; Keshavarz, T.; Roy, I. Polyhydroxyalkanoates: biodegradable polymers with a range of applications. *J. Chem. Technol. Biotechnol.* **2007**, *82*, 233–247. (b) Brannigan, R. P.; Dove, A. P. Synthesis, properties and biomedical applications of hydrolytically degradable materials based on aliphatic polyesters and polycarbonates. *Biomater. Sci.* **2017**, *5*, 9–21.
- (3) For selected heteroselective catalysts, see: (a) Ma, H.; Spaniol, T. P.; Okuda, J. Highly Heteroselective ring-opening polymerization of *rac*-lactide initiated by bis(phenolato)scandium complexes. *Angew. Chem., Int. Ed.* **2006**, *45*, 7818–7821. (b) Chmura, A. J.; Davidson, M. G.; Frankis, C. J.; Jones, M. D.; Lunn, M. D. Highly active and stereoselective zirconium and hafnium alkoxide initiators for solvent-free ring-opening polymerization of *rac*-lactide. *Chem. Commun.* **2008**, *11*, 1293–1295. (c) Zelikoff, A. L.; Kopilov, J.; Goldberg, I.; Coates, G. W.; Kol, M. New facets of an old ligand: titanium and zirconium complexes of phenylenediamine bis(phenolate) in lactide polymerisation catalysis. *Chem. Commun.* **2009**, *44*, 6804–6806. (d) Sergeeva, E.; Kopilov, J.; Goldberg, I.; Kol, M. Dithiodiolate ligands: Group 4 complexes and application in lactide polymerization. *Inorg. Chem.* **2010**, *49*, 3977–3979. (e) Bouyahy, M.; Ajellal, N.; Kirillov, E.; Thomas, C.; Carpentier, J. F. Exploring electronic versus steric effects in stereoselective ring-opening polymerization of lactide and β -butyrolactone with amino-alkoxy-bis(phenolate)-yttrium complexes. *Chem. - Eur. J.* **2011**, *17*, 1872–1883. (f) Maudoux, N.; Roisnel, T.; Carpentier, J. F.; Sarazin, Y. Aluminum, indium, and mixed yttrium-lithium complexes supported by a chiral binap-based fluorinated dialkoxide: Structural features and heteroselective ROP of lactide.

Organometallics **2014**, *33*, 5740–5748. (g) Yang, S.; Nie, K.; Zhang, Y.; Xue, M.; Yao, Y.; Shen, Q. New [ONOO]-type amine bis(phenolate) ytterbium(II) and -(III) complexes: Synthesis, structure, and catalysis for highly heteroselective polymerization of *rac*-lactide. *Inorg. Chem.* **2014**, *53*, 105–115. (h) Kremer, A. B.; Osten, K. M.; Yu, L.; Ebrahimi, T.; Aluthge, D. C.; Mehrkhodavandi, P. Dinucleating ligand platforms supporting indium and zinc catalysts for cyclic ester polymerization. *Inorg. Chem.* **2016**, *55*, 5365–5374.

(4) For selected isoselective catalysts, see: (a) Zhong, Z.; Dijkstra, P. J.; Feijen, J. Controlled and Stereoselective Polymerization of Lactide: Kinetics, Selectivity, and Microstructures. *J. Am. Chem. Soc.* **2003**, *125*, 11291–11298. (b) Nomura, N.; Ishii, R.; Yamamoto, Y.; Kondo, T. Stereoselective Ring-opening Polymerization of a Racemic Lactide by Using Achiral Salen- and Homosalen-Aluminum Complexes. *Chem. - Eur. J.* **2007**, *13*, 4433–4451. (c) Nomura, N.; Hasegawa, J.; Ishii, R. A Direct Function Relationship between Isotacticity and Melting Temperature of Multiblock Stereocopolymer Poly(*rac*-lactide). *Macromolecules* **2009**, *42*, 4907–4909. (d) Aluthge, D. C.; Patrick, B. O.; Mehrkhodavandi, P. A highly active and site selective indium catalyst for lactide polymerization. *Chem. Commun.* **2013**, *49*, 4295–4297. (e) Maudoux, N.; Roisnel, T.; Dorcet, V.; Carpentier, J. F.; Sarazin, Y. Chiral (1, 2)-Diphenylethylene-Salen Complexes of Tritel Metals: Coordination Patterns and Mechanistic Considerations in the Isoselective ROP of Lactide. *Chem. - Eur. J.* **2014**, *20*, 6131–6147. (f) Jones, M. D.; Hancock, S. L.; McKeown, P.; Schafer, P. M.; Buchard, A.; Thomas, L. H.; Mahon, M. F.; Lowe, J. P. Zirconium complexes of bipyrrrolidine derived salen ligands for the isoselective polymerization of *rac*-lactide. *Chem. Commun.* **2014**, *50*, 15967–15970. (g) Abbina, S.; Du, G. Zinc-catalyzed highly isoselective ring opening polymerization of *rac*-lactide. *ACS Macro Lett.* **2014**, *3*, 689–692. (h) Aluthge, D. C.; Ahn, J. M.; Mehrkhodavandi, P. Overcoming aggregation in indium salen catalysts for isoselective lactide polymerization. *Chem. Sci.* **2015**, *6*, 5284–5292. (i) Dai, Z.; Sun, Y.; Xiong, J.; Pan, X.; Wu, J. Alkali-metal monophenolates with a sandwich-type catalytic center as catalysts for highly isoselective polymerization of *rac*-lactide. *ACS Macro Lett.* **2015**, *4*, 556–560. (j) Xiong, J.; Zhang, J.; Sun, Y.; Dai, Z.; Pan, X.; Wu, J. Iso-selective ring-opening polymerization of *rac*-lactide catalyzed by crown ether complexes of sodium and potassium naphthalenolates. *Inorg. Chem.* **2015**, *54*, 1737–1743. (k) Rosen, T.; Popowski, Y.; Goldberg, I.; Kol, M. Zinc complexes of sequential tetradentate monoanionic ligands in the isoselective polymerization of *rac*-lactide. *Chem. - Eur. J.* **2016**, *22*, 11533–11536. (l) McKeown, P.; Davidson, M. G.; Kociok-Kohn, G.; Jones, M. D. Aluminium salalens vs. salans: “Initiator Design” for the isoselective polymerization of *rac*-lactide. *Chem. Commun.* **2016**, *52*, 10431–10434.

(5) For the selected rare-earth-catalyzed polymerization of *rac*-lactide, see: (a) Ma, H. Y.; Spaniol, T. P.; Okuda, J. Highly heteroselective ring-opening polymerization of *rac*-lactide initiated by bis(phenolato)scandium complexes. *Angew. Chem., Int. Ed.* **2006**, *45*, 7818–7821. (b) Amgoune, A.; Thomas, C. M.; Roisnel, T.; Carpentier, J. F. Ring-opening polymerization of lactide using Group 3 metal complexes supported by dianionic alkoxy-amino-bis(phenolate) ligands: Combining high activity, productivity, and selectivity. *Chem. - Eur. J.* **2006**, *12*, 169–179. (c) Platel, R. H.; Hodgson, L. M.; White, A. J. P.; Williams, C. K. Synthesis and characterization of a series of bis(oxo/thiophosphinic)diamido yttrium complexes and their application as initiators for lactide ring-opening polymerization. *Organometallics* **2007**, *26*, 4955–4963. (d) Platel, R. H.; White, A. J. P.; Williams, C. K. A Series of bis(phosphinic)diamido yttrium complexes as initiators for lactide polymerization. *Inorg. Chem.* **2008**, *47*, 6840–6849. (e) Hodgson, L. M.; Platel, R. H.; White, A. J. P.; Williams, C. K. A series of bis(thiophosphinic amido)yttrium initiators for lactide ring-opening polymerization. *Macromolecules* **2008**, *41*, 8603–8607. (f) Grunova, E.; Kirillov, E.; Roisnel, T.; Carpentier, J. F. Group 3 metal complexes of salen-like fluorinated dialkoxy-diimino ligands: Synthesis, structure and application in ring-opening polymerization of *rac*-lactide and *rac*- β -butyrolactone. *Organometallics* **2008**, *27*, 5691–5698. (g) Arnold, P.

L.; Buffet, J. C.; Blaudeck, R. P.; Sujecki, S.; Blake, A. J.; Wilson, C. C₃-symmetric lanthanide tris(alkoxide) complexes formed by preferential complexation and their stereoselective polymerization of *rac*-lactide. *Angew. Chem., Int. Ed.* **2008**, *47*, 6033–6036. (h) Platel, R. H.; White, A. J. P.; Williams, C. K. Stereocontrolled lactide polymerisation determined by the nuclearity of the yttrium initiator. *Chem. Commun.* **2009**, *27*, 4115–4117. (i) Mahrova, T. V.; Fukin, G. K.; Cherkasov, A. V.; Trifonov, A. A.; Ajellal, N.; Carpentier, J. F. Yttrium complexes supported by linked bis(amide) ligand: Synthesis, structure and catalytic activity in the ring-opening polymerization of cyclic esters. *Inorg. Chem.* **2009**, *48*, 4258–4266. (j) Broderick, E. M.; Diaconescu, P. L. Cerium(IV) catalysts for the ring-opening polymerization of lactide. *Inorg. Chem.* **2009**, *48*, 4701–4706. (k) Nie, K.; Gu, X.; Yao, Y.; Zhang, Y.; Shen, Q. Synthesis and characterization of amine bridged bis(phenolate) lanthanide aryloxides and their application in the polymerization of lactide. *Dalton Trans.* **2010**, *39*, 6832–6840. (l) Zhao, W.; Cui, D.; Liu, X.; Chen, X. Facile synthesis of hydroxyl-ended, highly stereoregular, star-shaped poly(lactide) from immortal ROP of *rac*-lactide and kinetics study. *Macromolecules* **2010**, *43*, 6678–6684. (m) Buffet, J. C.; Kapelski, A.; Okuda, J. Stereoselective polymerization of *meso*-lactide: Syndiotactic polylactide by heteroselective initiators based on trivalent metals. *Macromolecules* **2010**, *43*, 10201–10203. (n) Xu, T.; Yang, G.; Liu, C.; Lu, X. Highly robust yttrium bis(phenolate) ether catalysts for excellent isoselective ring-opening polymerization of racemic lactide. *Macromolecules* **2017**, *50*, 515–522.

(6) (a) Liu, X.; Shang, X.; Tang, T.; Hu, N.; Pei, F.; Cui, D.; Chen, X.; Jing, X. Achiral lanthanide alkyl complexes bearing N,O multidentate ligands. synthesis and catalysis of highly heteroselective ring-opening polymerization of *rac*-lactide. *Organometallics* **2007**, *26*, 2747–2757. (b) Amgoune, A.; Thomas, C. M.; Carpentier, J. F. Controlled ring-opening polymerization of lactide by group 3 metal complexes. *Pure Appl. Chem.* **2007**, *79*, 2013–2030. (c) Amgoune, A.; Thomas, C. M.; Carpentier, J. F. Yttrium complexes as catalysts for living and immortal polymerization of lactide to highly heterotactic PLA. *Macromol. Rapid Commun.* **2007**, *28*, 693–697. (d) Zhao, W.; Cui, D.; Liu, X.; Chen, X. Facile synthesis of hydroxyl-ended, highly stereoregular, star-shaped poly(lactide) from immortal ROP of *rac*-lactide and kinetics study. *Macromolecules* **2010**, *43*, 6678–6684.

(7) For the rare-earth-catalyzed polymerization of *rac*- β -butyrolactone, see: (a) Amgoune, A.; Thomas, C. M.; Ilinca, S.; Roisnel, T.; Carpentier, J. F. Highly active, productive, and syndiospecific yttrium initiators for the polymerization of racemic β -butyrolactone. *Angew. Chem., Int. Ed.* **2006**, *45*, 2782–2784. (b) Ajellal, N.; Bouyahyi, M.; Amgoune, A.; Thomas, C. M.; Bondon, A.; Pillin, I.; Grohens, Y.; Carpentier, J. F. Syndiotactic-enriched poly(3-hydroxybutyrate)s via stereoselective ring-opening polymerization of racemic β -butyrolactone with discrete yttrium catalysts. *Macromolecules* **2009**, *42*, 987–993. (c) Ajellal, N.; Durieux, G.; Delevoye, L.; Tricot, G.; Dujardin, C.; Thomas, C. M.; Gauvin, R. M. Polymerization of racemic β -butyrolactone using supported catalysts: a simple access to isotactic polymers. *Chem. Commun.* **2010**, *46*, 1032–1034. (d) Fang, J.; Tschan, M. J.-L.; Roisnel, T.; Trivelli, X.; Gauvin, R. M.; Thomas, C. M.; Maron, L. Yttrium catalysts for syndiospecific β -butyrolactone polymerization: on the origin of ligand-induced stereoselectivity. *Polym. Chem.* **2013**, *4*, 360–367. (e) Zhuo, Z.; Zhang, C.; Luo, Y.; Wang, Y.; Yao, Y.; Yuan, D.; Cui, D. Stereo-selectivity switchable ROP of *rac*- β -butyrolactone initiated by salen-ligated rare-earth metal amide complexes: the key role of the substituents on ligand frameworks. *Chem. Commun.* **2018**, *54*, 11998–12001.

(8) (a) Cao, T. P. A.; Buchard, A.; Le Goff, X. F.; Auffrant, A.; Williams, C. K. Phosphasalens yttrium complexes: highly active and stereoselective initiators for lactide polymerization. *Inorg. Chem.* **2012**, *51*, 2157–2169. (b) Bakewell, C.; Cao, T. P. A.; Long, N.; Le Goff, X. F.; Auffrant, A.; Williams, C. K. Yttrium phosphasalens initiators for *rac*-lactide polymerization: Excellent rates and high iso-selectivities. *J. Am. Chem. Soc.* **2012**, *134*, 20577–20580. (c) Bakewell, C.; Cao, T. P. A.; Le Goff, X. F.; Long, N. J.; Auffrant, A.; Williams, C. K. Yttrium phosphasalens initiators for *rac*-lactide polymerization. *Organometallics*

2013, 32, 1475–1483. (d) Bakewell, C.; White, A. J. P.; Long, N. J.; Williams, C. K. Metal-size influence in iso-selective lactide polymerization. *Angew. Chem., Int. Ed.* **2014**, 53, 9226–9230.

(9) (a) Whitelaw, E. L.; Jones, M. D.; Mahon, M. F. Group 4 salalen complexes and their application for the ring-opening polymerization of *rac*-lactide. *Inorg. Chem.* **2010**, 49, 7176–7181. (b) Whitelaw, E. L.; Davidson, M. G.; Jones, M. D. Group 4 salalen complexes for the production and degradation of polylactide. *Chem. Commun.* **2011**, 47, 10004–10006. (c) Whitelaw, E. L.; Loraine, G.; Mahon, M. F.; Jones, M. D. Salalen aluminium complexes and their exploitation for the ring opening polymerisation of *rac*-lactide. *Dalton Trans.* **2011**, 40, 11469–11473. (d) Pilone, A.; Press, K.; Goldberg, I.; Kol, M.; Mazzeo, M.; Lamberti, M. Gradient isotactic multiblock polylactides from aluminum complexes of chiral salalen ligands. *J. Am. Chem. Soc.* **2014**, 136, 2940–2943. (e) Stopper, A.; Rosen, T.; Venditto, V.; Goldberg, I.; Kol, M. Group 4 metal complexes of phenylene-salalen ligands in *rac*-lactide polymerization giving high molecular weight stereoblock poly(lactic acid). *Chem. - Eur. J.* **2017**, 23, 11540–11548. (f) Duan, Y. L.; Hu, Z. J.; Yang, B. Q.; Ding, F. F.; Wang, W.; Huang, Y.; Yang, Y. Zirconium and hafnium complexes bearing pyrrolidine derived salalen-type {ONNO} ligands and their application for ring-opening polymerization of lactides. *Dalton Trans.* **2017**, 46, 11259–11270. (g) Driscoll, O. J.; Leung, C. K. C.; Mahon, M. F.; McKeown, P.; Jones, M. D. Iron(III) Salalen Complexes for the Polymerisation of Lactide. *Eur. J. Inorg. Chem.* **2018**, 2018 (47), 5129–5135. (h) Britton, L.; Ditz, D.; Beament, J.; McKeown, P.; Quilter, H. C.; Riley, K.; Mahon, M. F.; Jones, M. D. Salalens and Salans Derived from 3-Aminopyrrolidine: Aluminium Complexation and Lactide Polymerization. *Eur. J. Inorg. Chem.* **2019**, 2019 (22), 2768–2773.

(10) Nakano, K.; Nakamura, M.; Nozaki, K. Alternating copolymerization of cyclohexene oxide with carbon dioxide catalyzed by (salalen)CrCl complexes. *Macromolecules* **2009**, 42, 6972–6980.

(11) (a) Press, K.; Cohen, A.; Goldberg, I.; Venditto, V.; Mazzeo, M.; Kol, M. Salalen titanium complexes in the highly isospecific polymerization of 1-hexene and propylene. *Angew. Chem., Int. Ed.* **2011**, 50, 3529–3532. (b) Li, S.; Zhu, Y.; Liang, H.; Xie, X.; Zhan, Y.; Liang, G.; Zhu, F. The influences of electronic effect and isomerization of salalen titanium(IV) complexes on ethylene polymerization in the presence of methylaluminoxane. *RSC Adv.* **2019**, 9, 41824–41831.

(12) (a) Stopper, A.; Okuda, J.; Kol, M. Ring-opening polymerization of lactide with Zr complexes of {ONSO} ligands: From heterotactically inclined to isotactically inclined Poly(lactic acid). *Macromolecules* **2012**, 45, 698–704. (b) Stopper, A.; Press, K.; Okuda, J.; Goldberg, I.; Kol, M. Zirconium complexes of phenylene-bridged {ONSO} ligands: coordination chemistry and stereoselective polymerization of *rac*-lactide. *Inorg. Chem.* **2014**, 53, 9140–9150. (c) Han, B.; Zhang, L.; Kyran, S. J.; Liu, B. Y.; Duan, Z. Y.; Darensbourg, D. J. Copolymerization of carbon dioxide and cyclohexene oxide catalyzed by chromium complexes bearing semirigid [ONSO]-type ligands. *J. Polym. Sci., Part A: Polym. Chem.* **2016**, 54, 1938–1944. (d) Stewart, J. A.; McKeown, P.; Driscoll, O. J.; Mahon, M. F.; Ward, B. D.; Jones, M. D. Tuning the thiolen: Al(III) and Fe(III) thiolen complexes for the isoselective ROP of *rac*-lactide. *Macromolecules* **2019**, 52, 5977–5984.

(13) (a) Cao, T. P. A.; Labouille, S.; Auffrant, A.; Jean, Y.; Le Goff, X. F.; Le Floch, P. Pd(II) and Ni(II) complexes featuring a “phosphasalen” ligand: synthesis and DFT study. *Dalton Trans.* **2011**, 40, 10029–10037. (b) Demange, M.; Boubekeur, L.; Auffrant, A.; Mezaïlles, N.; Ricard, L.; Le Goff, X.; Le Floch, P. A new and convenient approach towards bis(iminophosphoranyl)methanelligands and their dicationic, cationic, anionic and dianionic derivatives. *New J. Chem.* **2006**, 30, 1745–1754. (c) Cheisson, T.; Cao, T. P. A.; Le Goff, X. F.; Auffrant, A. Nickel complexes featuring iminophosphorane-phenoxide ligands for catalytic ethylene dimerization. *Organometallics* **2014**, 33, 6193–6199. (d) Jian, Z.; Petrov, A. R.; Hangaly, N. K.; Li, S.; Rong, W.; Mou, Z.; Rufanov, K. A.; Harms, K.; Sundermeyer, J.; Cui, D. Phosphazene-functionalized cyclopentadienyl and its derivatives ligated rare-earth metal alkyl complexes: synthesis, structures,

and catalysis on ethylene polymerization. *Organometallics* **2012**, 31, 4267–4282. (e) Xie, H.; Mou, Z.; Liu, B.; Rong, W.; Li, S.; Cui, D. Phosphinimino-amino magnesium complexes: synthesis and catalysis of heteroselective ROP of *rac*-lactide. *Organometallics* **2014**, 33, 722–730. (f) Welch, G. C.; Piers, W. E.; Parvez, M.; McDonald, R. Neutral and cationic organoaluminum complexes utilizing a novel anilido-phosphinimine ancillary ligand. *Organometallics* **2004**, 23, 1811–1818. (g) Johnson, K. R. D.; Hayes, P. G. Synthesis and reactivity of dialkyl lutetium complexes supported by a novel bis(phosphinimine)carbazole pincer ligand. *Organometallics* **2009**, 28, 6352–6361.

(14) (a) Broderick, E. M.; Guo, N.; Vogel, C. S.; Xu, C.; Sutter, J.; Miller, J. T.; Meyer, K.; Mehrkhodavandi, P.; Diaconescu, P. L. Redox control of a ring-opening polymerization catalyst. *J. Am. Chem. Soc.* **2011**, 133, 9278–9281. (b) Broderick, E. M.; Guo, N.; Wu, T.; Vogel, C. S.; Xu, C.; Sutter, J.; Miller, J. T.; Meyer, K.; Cantat, T.; Diaconescu, P. L. Redox control of a polymerization catalyst by changing the oxidation state of the metal center. *Chem. Commun.* **2011**, 47, 9897–9899. (c) Myers, D.; White, A. J. P.; Forsyth, C. M.; Bown, M.; Williams, C. K. Phosphasalen indium complexes showing high rates and isoselectivities in *rac*-lactide polymerizations. *Angew. Chem., Int. Ed.* **2017**, 56, 5277–5282. (d) Thevenon, A.; Cyriac, A.; Myers, D.; White, A. J. P.; Durr, C. B.; Williams, C. K. Indium catalysts for low-pressure CO₂/epoxide ring-opening copolymerization: Evidence for a mononuclear mechanism? *J. Am. Chem. Soc.* **2018**, 140, 6893–6903.

(15) Nie, K.; Gu, W.; Yao, Y.; Zhang, Y.; Shen, Q. Synthesis and characterization of salalen lanthanide complexes and their application in the polymerization of *rac*-lactide. *Organometallics* **2013**, 32, 2608–2617.

(16) Matsumoto, K.; Oguma, T.; Katsuki, T. Highly enantioselective epoxidation of styrenes catalyzed by proline-derived C₁-symmetric Titanium(Salalen) Complexes. *Angew. Chem., Int. Ed.* **2009**, 48, 7432–7435.

(17) (a) Yu, I.; Acosta-Ramirez, A.; Mehrkhodavandi, P. Mechanism of living lactide polymerization by binuclear indium catalysts and its impact on isoselectivity. *J. Am. Chem. Soc.* **2012**, 134, 12758–12773. (b) Osten, K. M.; Mehrkhodavandi, P. Indium catalysts for ring opening polymerization: Exploring the importance of catalyst aggregation. *Acc. Chem. Res.* **2017**, 50, 2861–2869.

(18) (a) Dube, T.; Gambarotta, S.; Yap, G. Preparation and reactivity of a compartmental schiff-base samarium binuclear complex. *Organometallics* **1998**, 17, 3967–3973. (b) Zheng, Z. Ligand-controlled self-assembly of polynuclear lanthanide-oxo/hydroxo complexes: from synthetic serendipity to rational supramolecular design. *Chem. Commun.* **2001**, 24, 2521–2529. (c) Korobkov, I.; Arunachalampillai, A.; Gambarotta, S. Cyclometalation and solvent deoxygenation during reduction of a homoleptic Th(OAr)₄ complex: serendipitous formation of a terminally bonded Th–OH function. *Organometallics* **2004**, 23, 6248–6252.